Applied Thermal Engineering 280 (2025) 128121

Contents lists available at ScienceDirect

Applied Thermal Engineering

journal homepage: www.elsevier.com/locate/apthermeng

Research Paper

Refined kinetic mechanism for modeling ammonia combustion in air assisted by nanosecond discharged plasma☆

Zubair Ali Shah [a,*], Giacomo Cinieri [a], Mingming Zhu [b], Muhammad Basit Chandio [a], Maria Grazia De Giorgi [a,*]

[a] University of Salento, Dep. Engineering for Innovation, Via per Monteroni, 73100 Lecce, Italy
[b] Faculty of Engineering and Applied Sciences, Cranfield University, Cranfield, Bedfordshire, MK 43 0AL, United Kingdom

ARTICLE INFO

Keywords:
Ammonia
Combustion
Nanosecond plasma discharge
Ignition delay time
Laminar flame speed

ABSTRACT

This study explores the effects of Nanosecond Pulsed Discharge Plasma (NSPD) on the ignition and flame propagation characteristics of ammonia (NH_3)/air mixtures at low and intermediate temperatures under atmospheric pressure. A newly developed and validated plasma-assisted kinetic mechanism is proposed to evaluate both Ignition Delay Time (IDT) and Laminar Flame Speed (LFS) across a range of temperatures and equivalence ratios. Results show that plasma significantly reduces IDT and enhances LFS by generating excited species and radicals, such as H, O, OH, NH_2, and $O(^1D)$, that accelerate reaction pathways and enable earlier chain-branching. The effect is most pronounced at low temperatures ($T < 950$ K), where thermal chemistry is limited, and plasma-induced kinetics play a dominant role. Sensitivity analyses reveal that reactions involving NH_2 and H atoms are the most impactful in reducing IDT, with $NH_2 + NO \rightleftharpoons NNH + OH$ emerging as the key pathway, especially under plasma conditions. The role of H atoms also becomes up to three times more significant in the presence of plasma. For LFS, the chain-branching reaction $H + O_2 \rightleftharpoons OH + O$ is consistently the most influential, with plasma further amplifying its contribution. The maximum LFS is observed at $\Phi \approx 1.1$, for both plasma and non-plasma cases, however, plasma-induced enhancements are more evident at lean equivalence ratios ($\Phi = 0.8$), where the additional radicals generated by NSPD have the greatest relative impact. At stoichiometric and rich conditions ($\Phi \geq 1.0$), thermal activation prevails and the plasma effect becomes marginal. Overall, the study demonstrates that NSPD is a promising strategy to enable and control low-temperature ammonia combustion by actively modulating ignition chemistry and flame dynamics.

1. Introduction

Among the numerous greenhouse gases, carbon dioxide (CO_2) produced by fossil fuel combustion is the main driver of global warming [1]. In order to face this challenge, most countries across the world are undertaking considerable steps to transform their energy systems to cleaner and more sustainable [2,3,4]. Ammonia has emerged as a promising candidate to help mitigate the impending energy crisis. It is gaining widespread attention for its role as a carbon-free energy carrier and a high-density hydrogen energy vector. Beyond its energy properties, ammonia holds appeal for diverse industries due to its well-developed storage and transportation infrastructures, making long-term storage both feasible and cost-effective [5]. Despite its many advantages, ammonia faces several challenges that need to be overcome before it can be directly used in combustion devices such as turbines, compression ignition (CI), and spark ignition (SI) engines. These obstacles encompass factors such as slow flame speed, resistance to auto-ignition [6], high NOx emission, and narrow flammability range.

In recent review papers [7,8,9], ammonia is considered a promising fuel for the future, emphasizing the importance of addressing these key challenges for its effective integration. To establish ammonia as a viable future fuel, a thorough understanding of its oxidation processes is necessary. Given its low reactivity, earlier investigations have investigated the oxidation of pure NH_3 under high and intermediate temperatures [10,11], or in blends with various fuels, including H_2 [12,13,14], syngas [15], and diesel [16]. These studies highlight the impact of a fuel blending strategy in enhancing key parameters like LFS, flammability range, and autoignition behavior of ammonia. Various solutions to

☆ This article is part of a special issue entitled: 'Combustion for Net-Zero' published in Applied Thermal Engineering.

* Corresponding authors.
E-mail addresses: zubairali.shah@unisalento.it (Z.A. Shah), mariagrazia.degiorgi@unisalento.it (M.G. De Giorgi).

https://doi.org/10.1016/j.applthermaleng.2025.128121
Received 4 March 2025; Received in revised form 3 August 2025; Accepted 29 August 2025
Available online 11 September 2025
1359-4311/© 2025 The Author(s). Published by Elsevier Ltd. This is an open access article under the CC BY license (http://creativecommons.org/licenses/by/4.0/).

address the challenges of ammonia combustion have been proposed in the literature. One popular method is blending with H_2. The addition of H_2 augments the reactivity of NH_3 combustion across all conditions, leading to an enhancement in burning velocity. This improvement primarily arises from chemical effects attributed to the reduction in chemical activation energy and transport effects facilitated by the high mobility of H_2. Moreover, elevating pressure and increasing H_2 addition ratios can substantially reduce ignition delay time of NH_3 mixtures, further promoting the ignition of NH_3 [17]. While ongoing research on blended fuels appears promising in mitigating certain challenges associated with traditional ammonia combustion, the production of H_2 remains a formidable task. Given that ammonia inherently serves as a hydrogen carrier, investigations are underway regarding the cracking of ammonia to generate H_2. However, a significant difficulty in the cracking process lies in the demand for a substantial surface area-to-volume ratio for catalyst-based decomposition.

Recently, non-equilibrium plasma has been proposed to address the challenges associated with ammonia combustion [9]. Non-equilibrium plasma is recognized for its ability to create distinctive chemical pathways, promoting fuel pyrolysis, generating O radicals, and achieving ultra-fast heating, thereby accelerating reaction rates. Numerous studies have explored the impact of non-equilibrium plasma on NH_3 combustion, employing both experimental [18,19,20] and numerical [21,22,23,24] approaches. Choe et al. [18] carried out the first experimental study on plasma-assisted ammonia combustion, and their findings demonstrated that plasma not only reduces NOx emissions in ammonia flames but also extends the lean blowoff limits. Kim et al. [19] experimentally studied the effects of non-thermal plasma (NTP) on NH_3/air flames and NOx emissions in a gas turbine combustor. Results show that NTP enhances flame stability and extends the stable combustion regime. Additionally, NTP significantly reduces NOx emissions, particularly through the NH_2 reactions, as confirmed by NH chemiluminescence measurements. Tang et al. [20] investigated the flammability and NOx emissions of swirling NH_3/air flames via AC-driven gliding arc discharges. The findings show that plasma discharges expanded the lean blow-off limit by 0.3–0.4 and stabilized flames even at low equivalence ratios. The detachment and blow-off limits improved with increasing airflow, and the plasma effectively stabilized lean flames while slightly reducing NOx emissions, especially at higher equivalence ratios (>0.75). Galia Faingold and Joseph K. Lefkowitz [21] performed numerical simulations to study the ignition limits of NH_3/O_2/He in a non-thermal plasma (NTP) across temperatures of 600–1500 K and varying numbers of pulses and pulse frequencies. By integrating a 0-D plasma solver (ZDPlasKin) with CHEMKIN software, they found that IDT can be reduced by 40–60 % with a moderate number of pulses and that higher pulse repetition frequencies also lead to shorter IDTs. Akira Shioyoke et al. [22] studied the effects of NTP on the laminar burning velocity of ammonia flames, and their findings show that as the reduced electric field (E/N) increases, the rate of ammonia decomposition accelerates, which significantly enhances the burning velocity. This improvement is primarily attributed to the increased production of H by plasma discharge, which plays a crucial role in boosting the combustion process. Taneja et al. [23] investigated the impact of operating parameters on ignition delays and NOx emissions in plasma-assisted ammonia combustion in constant-volume and pressure reactors. Results showed that lean mixtures ignite faster than stoichiometric and rich mixtures due to lower consumption rates of OH radicals, but produce more NO due to increased oxygen radicals. Higher pressures led to longer ignition delays and reduced NO production, while the use of non-equilibrium plasma significantly decreased ignition delays and NOx emissions compared to traditional thermal methods, emphasizing the role of excited species and radicals in the combustion process. Mao et al. [24] investigated the plasma-assisted low-temperature ignition of NH_3/air and NOx formation, and the findings show that plasma discharge dramatically reduces IDT by 2–5 orders of magnitude compared to thermal ignition due to enhanced radical production. The analysis highlights that reactions involving O and electronically excited species are key to enhancing NH_3 ignition and that NOx formation through plasma also contributes to ignition improvement. Although valuable research efforts, the existing literature offers limited data and in-depth analyses on the effect of plasma discharge on IDT and LFS. Previous research has largely focused on the effects of plasma on the ignition delay time (IDT) of ammonia, leading to a scarcity of publicly available data on the influence of plasma discharge frequency on the laminar flame speed (LFS) of ammonia flames. To fill these gaps in this study, a validated plasma mechanism was employed to simulate plasma discharge processes, and a new combustion mechanism was developed and validated across low to intermediate temperature ranges for IDT and LFS. Then we examine the impact of key plasma parameters on both IDT and LFS for an NH_3/air mixture at low to intermediate temperatures under atmospheric pressure.

2. Numerical methodology

Numerical modeling was conducted by integrating a 0D plasma kinetic model (ZDPlasKin) [25] and the chemical kinetic model (CHEMKIN) [26]. ZDPlasKin was utilized to analyze the NSPD, and CHEMKIN was considered to predict the IDT and LFS.

Due to the distinct time scales involved, the plasma-enhanced combustion process is divided into separate discharge and combustion phases.

The discharge phase typically occurs on a time scale of nanoseconds (ns) to microseconds (μs), often in the range of 10^{-9} to 10^{-6} s, depending on the pulse duration and reduced electric field (E/N) applied during the plasma discharge.

Conversely, the combustion phase takes place on significantly longer time scales, usually in the order of milliseconds (ms) to seconds (s), depending on the reactant composition, temperature, and pressure conditions.

The discharge phase is characterized by energy transfer and the activation of active and excited species. A significant number of active and excited species are generated after a series of events that include particle excitation, charge exchange, ionization, dissociation, excited particle quenching, and electron–ion recombination [27]. The output from the ZDPlasKin was used as input for the combustion process of the NH_3/air mixture in the combustion stage, simulating the whole process of plasma-enhanced ammonia combustion.

In this study, two distinct reactor models were implemented to investigate the combustion process: the 0D Closed Homogeneous Batch Reactor (CHBR) for IDT calculations and the Premixed Laminar Flame Speed Reactor (PLFSR) for LFS calculations.

The PLFSR in CHEMKIN is a one-dimensional, steady-state model designed to compute the laminar flame speed of premixed fuel–air mixtures under constant pressure conditions [28]. The system is formulated as an eigenvalue problem, where the flame speed is solved such that the conservation equations and boundary conditions are simultaneously satisfied. The governing equations include species mass conservation, energy conservation, and continuity. The numerical solution is obtained using finite difference discretization over an adaptive spatial grid, and solved iteratively via Newton-Raphson or shooting methods. The flame speed is adjusted to satisfy the boundary conditions at the burnt gas side, where the temperature and composition reach equilibrium.

The IDT was determined using CHEMKIN's Closed Homogeneous Batch Reactor (CHBR) model. In this approach, the simulated IDT is defined as the time from the start of the simulation until the temperature gradient reaches its maximum value. The CHBR solver's relative and absolute error tolerances for the ODEs were set to 1.0×10^{-6} and 1.0×10^{-12}, respectively.

Preliminary simulations, i condition without plasma discharges and 1 atm and different initial temperatures, performed using both CV and CP configurations, as well as Plug Flow Reactor (PFR) models,

underlined that CV conditions lead to reduced IDTs because of pressure rise, while PFR simulations, despite being at constant pressure, showed shorter IDTs than CP as a result of transport effects and the spatial propagation of plasma-generated radicals.

For the remainder of this study, CP conditions were adopted because they represent a zero-dimensional, well-stirred system that approximates the thermodynamic behavior of many experimental configurations (e.g., rapid compression machines) and provide a consistent basis for both IDT and laminar flame speed analyses. Furthermore, CP simulations allow for direct control of pressure and temperature, isolate the chemical kinetic effects of plasma without additional pressure-rise or transport effects, and ensure numerical robustness for extensive parametric studies.

All simulations generated grid-independent solutions, which ensured the accuracy and reliability of the computational results for both IDT and LFS under the given circumstances. The general methodology can be summarized in the five steps shown in Fig. 1 using the numerical procedure flowchart.

Step 1: A thorough examination of literature was conducted to select a validated, detailed, and expanded version of the plasma kinetic mechanism by compiling electron collision cross-section data.

Step 2: The initial configuration of code and boundary conditions in ZDPlasKin for simulating plasma reactions involved specifying parameters such as temperature, pressure, E/N, and initial mixture composition. This process was accompanied by preparing a detailed reaction mechanism file for plasma chemistry and compiling the cross-section data file.

Step 3: ZDPlasKin plasma discharge simulations were run for a short period of time to investigate plasma effects for different pulse numbers, equivalence ratios, and E/N values to find the new composition of the mixture as a result of plasma discharge.

Step 4: The outcomes obtained from simulating plasma discharge, involving active and excited species such as H, OH, O, NH_2, NH, O_3, $O_2(a^1\Delta_g)$, and O (^{1}D), generated during the discharge, were incorporated into CHEMKIN to examine the combustion process.

Step 5: The updated version of the combustion mechanism, integrated into combustion reactor models, was employed to predict combustion enhancement. The 0D CHBR and PLFSR were utilized to analyze the effects of NSPD on the IDT and LFS of the NH_3/air mixture, respectively.

2.1. Details of the plasma and combustion kinetic mechanisms

2.1.1. Plasma kinetic mechanism

Simulations of plasma discharge are conducted using the validated Plasma Kinetic Mechanism [29]. The plasma mechanism was developed by combining the mechanism proposed by Faingold et al. [21] for NH_3/O_2/He, N_2 plasma reactions are referenced from Zhong et al. [30], while the electron-species interaction collision cross sections are obtained from the LX-Cat database [31]. Table 1 presents a comprehensive list of species, including charged particles, excited states, and intermediates, as part of the detailed plasma mechanism. This mechanism includes charge exchanges, recombination, quenching, ionizations, excitations, and elementary reactions in the neutral state for NH_3, O_2, and N_2.

Table 1
A comprehensive plasma kinetic mechanism including all types of ammonia/air reactants, elements, active, exciting, and charged species.

Species category	Symbol
Elements	H, N, O, AR, HE, E
Thermal species	H, N, O, OH, NH, AR, HE, NO, HNO, NOH, NNH, HONO, HNOH, HNNO, H_2, O_2, N_2, O_3, NH_3, NH_2, H_2O, HO_2, H_2O_2, OH*, N_2O, NO_2, O_2 (1delta), N_2O_4, N_2O_3, NO_3, N_2H_4, N_2H_3, N_2H_2, HNO_3, H_2NO, NH_2OH
Plasma species	O_2 (A1), O_2 (B1), O_2 (4.5 eV), O(1S), O(1D), O_2^+, O^+, O_2*, He*, He^+, NH_3^+, H_3^+, NH_2^+, NH^+, N_2H^+, N_2^+, H_2^+, N^+, H^+, N_2(A), N_2(B), N_2(ab), N_2(C), N(2D), E

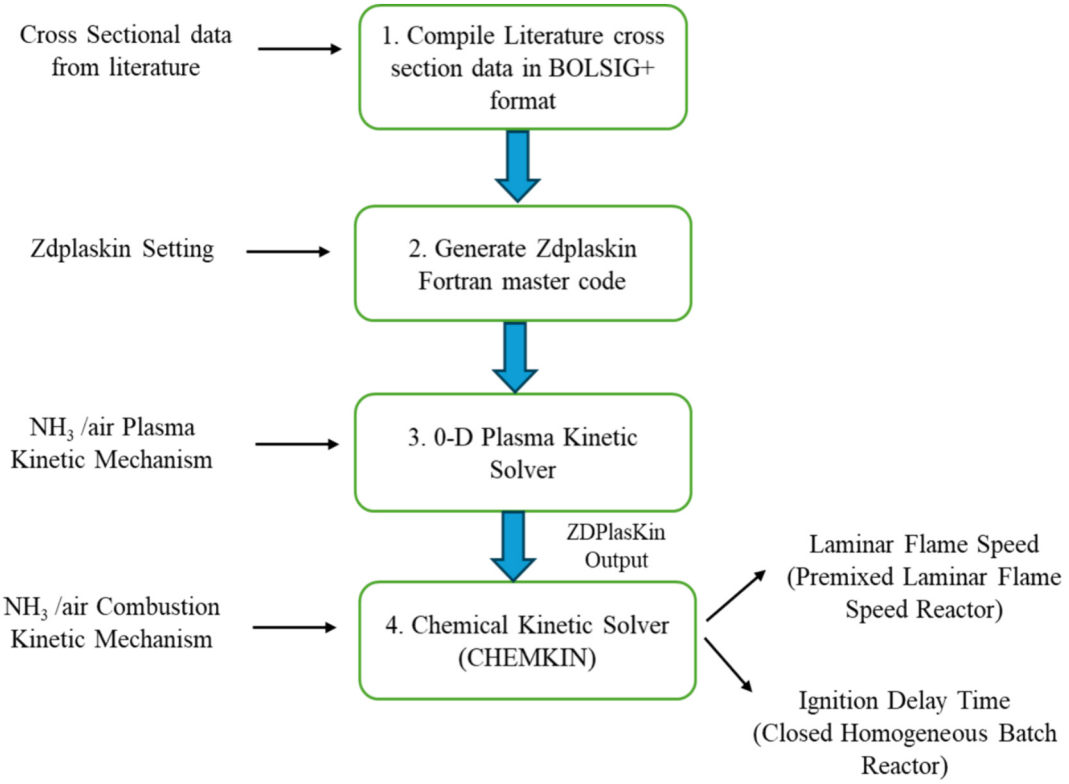


Fig. 1. A comprehensive diagram illustrates the numerical integration of ZDPlasKin and CHEMKIN.

2.1.2. Combustion kinetic mechanism

To enhance the mechanism and conduct simulations, an in-depth evaluation of NH_3 combustion mechanisms was carried out. The Mei mechanism [32] was chosen for modification and simulation due to its ability to more accurately capture flame speeds under various conditions and IDT [23,32] at high temperatures, within experimental uncertainty ranges. Furthermore, the Mei mechanism demonstrated greater accuracy in estimating NO levels in a jet-stirred reactor [33]. Therefore, it has been chosen as the reference combustion mechanism in this study for further refinement and validation across a wider temperature range, particularly under plasma-assisted conditions. The refinement strategy targeted three key aspects of the mechanism. First, the hydrogen reaction pathway in Mei's mechanism, which is primarily based on the work of Hashemi et al. [34], was enhanced by integrating several chemically termolecular reactions ($H + O_2 + O/OH/H = products$). These reactions, although not excluded in the Hashemi model, were explicitly included to improve the accuracy of LFS predictions for hydrogen, resulting in better alignment with experimental data and improved model fidelity in capturing flame speed behavior. Second, the NH_3 sub-mechanism and DeNOx pathways underwent substantial updates, particularly focusing on reactions relevant to NOx and HNO formation. These adjustments, based on recent experimental and numerical studies, aim to improve predictive accuracy across low-to-intermediate temperatures as well as in rich combustion environments. The modified reactions and rate constants are presented in Table 2, and the thermodynamic data of the species are modified based on the recent study of Glarborg et al. [35].

A novel aspect of the modified mechanism involves the inclusion of the ozone sub-mechanism and oxygen excited species chemistry. Excited species' reactions of oxygen, such as O (^1D), and O_2 ($a^1\Delta_g$) adopted from Konnov [55] and the O_3 sub-mechanism reactions from ZH Wang et al. [56] are added to investigate the effect of ozone because ozone and excited species of oxygen are produced during the plasma discharge and previous studies showed that they have a positive effect on LFS and IDT [57,58,59].

Chen et al. [57] demonstrated that the addition of ozone (O_3) considerably boosts the burning velocity of ammonia (NH_3) flames, especially on the fuel-lean side, achieving a maximum increase of 15.34 % at an equivalence ratio of 0.6 with 5000 ppm O_3. This enhancement is primarily attributed to active radicals such as HNO, generated from the decomposition of O_3, which facilitate the overall combustion process. Shah et al. [58] demonstrated that adding O_3 to the oxidizer significantly increases the LFS of ammonia/hydrogen/air mixtures. Specifically, the addition of a 0.01 mol fraction of O_3 produced effects comparable to a 10 % increase in hydrogen within the NH_3/air mixture, indicating that ozone can effectively boost NH_3 combustion performance under normal conditions. Stark et al. [59] studied the impact of singlet oxygen molecules $O_2(a^1\Delta_g)$ on laminar flame propagation in a methane-air mixture. They validated a kinetic model that includes electronically excited oxygen species, and findings showed that adding 10 % $O_2(a^1\Delta_g)$ significantly increased flame speed by a factor of 1.7 in a fuel-lean mixture due to enhanced chain reactions. In a fuel-rich mixture, the increase in flame speed was more modest, at a factor of 1.4.

In this study, LFS analysis was carried out to evaluate the impact of the additional reactions on the numerical stiffness of the mechanism compared to Mei's original mechanism. As a consequence of the increased chemical complexity, the computational time increased by approximately 33 %, indicating a moderate rise in stiffness while remaining within a manageable range for the simulations performed.

2.2. Validation analysis of the updated kinetic mechanism

A validation analysis was conducted to assess the accuracy of the present mechanism used in this study, comparing ignition delay times (IDT) and laminar flame speeds (LFS) with both experimental and numerical results.

To investigate the IDT of the NH_3/air mixture, various mechanisms,

Table 2
The revised and modified reactions and their rate constants are incorporated into the base Mei-Mech [32] model using the expression $k = A\,T^n \exp(-Ea/RT)$.

No.	Reaction	A	Ea	n	Ref.
R1	$NH_3 + M = NH_2 + H + M$	2.20E + 16	93,470	0.000	[36]
R2	$NH_3 + H = NH_2 + H_2$	2.89E + 06	1.04E + 04	2.230	[37]
R3	$NH_3 + OH = H_2O + NH_2$	1.56E + 05	118.9	2.372	[38]
R4	$NH_3 + HO_2 = NH_2 + H_2O_2$	1.173	17260.0	3.839	[38]
R5	$NH_3 + O = NH_2 + OH$	4.43E + 02	6739.9	3.180	[38]
R6	$NH_2 + OH = NH + H_2O$	3.30E + 06	−217	1.949	[39]
R7	$NH + H = N + H_2$	3.01E + 13	0.00	0.000	[40]
R8	$NH + NH = N_2 + H_2$	6.26E + 12	−160.9	−0.036	[39]
R9	$NH + NH = N_2 + H + H$	5.63E + 13	−160.9	−0.036	[39]
R10	$NH_2 + NO_2 = H_2NO + NO$	8.60E + 11	−1186	0.110	[41]
R11	$NH_2 + NO_2 = N_2O + H_2O$	2.20E + 11	−1186	0.110	[41]
R12	$NH + NO = N_2 + OH$	6.80E + 14	20	−0.780	[40]
R13	$NH + NO = N_2O + H$	2.70E + 15	20	−0.780	[40]
R14	$N_2O + H = N_2 + OH$ DUP	3.31E + 10	5090	0.000	[42]
	$N_2O + H = N_2 + OH$ DUP	7.83E + 14	19,390	0.000	
R15	N_2O (+ M) = N_2 + O (+ M) LOW/ N_2/ 1.7/ O_2/ 1.4/ H_2O/ 12.0/ NO/ 3.0/ N_2O / 3.5/	1.69E + 11	57,653	0.000	[43]
R16	$NO + H = NH + O$	9.90E + 14	69,900	−0.100	[44]
R17	$NH + O_2 = NO + OH$	2.01E + 16	5672	−1.380	[45]
R18	$N + OH = NO + H$	3.80E + 13	0.000	0.000	[46]
R19	$N + NO = N_2 + O$	9.40E + 12	0.000	0.140	[46]
R20	$NH_2 + O = HNO + H$ DUP	0.15E + 16	836.7	−0.547	[47]
	$NH_2 + O = HNO + H$ DUP	0.77E + 14	646.4	−0.277	
R21	$NH + OH = HNO + H$	3.20E + 14	−46	−0.376	[39]
R22	$NH + O_2 = HNO + O$	0.41E + 12	10,670	0.090	[45]
R23	$NH_2 + O_2 = HNO + OH$	2.90E-02	18,185	3.764	[48]
R24	$HNO = H + NO$	0.18E + 21	47,880	−3.008	[38]
R25	$HNO + OH = NO + H_2O$	7.20E + 13	0.000	0.000	[49]
R26	$HNO + O = NO + OH$	2.31E + 13	0.000	0.000	[50]
R27	$HONO + H = HNO + OH$	1.50E + 03	4600	2.700	[51]
R28	$NH_2 + O_2 = H_2NO + O$	2.60E + 11	2.91E + 04	0.487	[48]
R29	$NH_2 + HONO = NH_3 + NO_2$	4.84E + 00	−4.58E + 03	3.360	[52]
R30	$HONO + H = NO + H_2O$	4.30E + 09	4100	1.000	[51]
R31	$N_2H_2 + H = NNH + H_2$	1.10E + 14	3128	0.000	[41]
R32	$H + O_2 = O + OH$	1.37E1 + 3	1.44E + 04	0.2434	[53]

(continued on next page)

Table 2 (*continued*)

No.	Reaction	A	Ea	n	Ref.
R33	$O + H_2 = H + OH$	1.26E + 06	6956.9	2.2704	[53]
R34	$HO_2 + HO_2 = H_2O_2 + O_2$	1.93E-02	−4960	4.120	[54]
R35	$HO_2 + HO_2 = OH + OH + O_2$	6.41E + 17	8540	−1.540	[54]

including those by Otomo et al. [60], Han et al. [61], Okafor et al. [62], and Stagni et al. [63], were applied in numerical simulations using the CHEMKIN software [26]. The updated combustion mechanism was validated against experimental data [12] for intermediate temperature (1100 K to 1180 K), high pressure 60 bar, and different equivalence ratios as shown in Fig. 2. It was also validated with experimental data [64] for high temperatures (1600 K to 2000 K) and pressures of 1.2 atm and 10 atm, as shown in Fig. 3. In these figures, symbols represent experimental data, while lines indicate simulated results from the current and previous models. Figs. 2 and 3 illustrate that the predictions from the present and Otomo et al. [60] model show good agreement with experimental measurements across low and high-temperature ranges. However, the Han et al. [61] and Stagni et al. [63] models perform well at high temperatures but show significant deviations in IDT at low temperatures, while the Okafor et al. [62] model consistently overestimates IDT in all scenarios.

The mechanism was further validated for LFS at a pressure of 1 atm, across various equivalence ratios and initial temperatures, using experimental data from Shrestha et al. [65], as shown in Fig. 4. In this figure, symbols represent the experimental data, while lines depict the simulated results from the current model. Fig. 4 highlights that the model aligns well with the experimental data across all conditions, indicating its capability to accurately capture LFS behavior at different temperatures and equivalence ratios.

The literature lacks validated experimental data for LFS and IDT in the presence of plasma discharges on an ammonia/air mixture. However, a few numerical studies, most notably Shahsavari et al. [29], have provided reference values under conditions closely matching the present work. Therefore, we report in Fig. 5a below the analysis of laminar flame speed and ignition delay time for plasma-assisted $NH_3/O_2/N_2$ combustion at $\phi = 1$, Tin = 850 K, with a pulse repetition frequency (PRF) of 50 kHz and energy density Ep = 5 mJ/cm^3. Regarding the experimental data on plasma, simulations were performed to compute the water concentration calculated as a prediction for 30 kHz, 1500-nanosecond plasma pulses in a $0.1667H_2$ / $0.0833O_2$ / 0.75 He mixture at 8000 Pa [66] (Fig. 5b).

3. Results and Discussion

3.1. Effect of E/N on IDT and the production of the maximum mole fraction of species

The E/N ratio is widely recognized as a critical parameter influencing plasma discharge within the mixture. At higher E/N values, plasma effectively generates species such as H, O, OH, NH_2, NH, O_3, O_2 ($a^1\Delta_g$), and O(^{1}D), which in turn initiate new low-temperature reaction pathways that enhance NH_3 combustion at reduced temperatures. Fig. 6 shows the active and excited species produced during 20 plasma discharge pulses across different E/N levels.

Species such as H, O, NH, O_2 ($a^1\Delta_g$), and O(^{1}D) exhibit a clear increasing trend as E/N rises from 100 Td to 350 Td. This indicates that higher reduced electric fields enhance electron energy transfer efficiency, promoting ionization, dissociation, and excitation processes that produce these reactive species.

In contrast, OH, NH_2, and O_3 concentrations initially increase with rising E/N (peaking around 260–280 Td) but subsequently decrease at higher E/N levels. This non-monotonic behavior of OH, NH_2, and O_3 with increasing E/N can be attributed to the interplay of radical production, recombination, and precursor depletion. While species such as H, O, NH, O_2 ($a^1\Delta_g$), and O(^{1}D) show a sustained increase in mole fraction from 100 Td to 350 Td, reflecting enhanced electron energy transfer efficiency and activation of dissociation/excitation pathways OH, NH_2, and O_3 reach a peak around 260–280 Td and subsequently decline. This trend results from: (i) increased radical recombination (e.g., $H + OH \rightarrow H_2O$, $O + O_3 \rightarrow 2O_2$), (ii) progressive depletion of precursor molecules such as NH_3, H_2O, and O_2 due to intensified electron impact dissociation, and (iii) quenching of electronically excited species (e.g., O(^{1}D), O_2 ($a^1\Delta_g$)), which limits their contribution to chain-propagating reactions.

These findings are consistent with the numerical results reported by Shahsavari et al.(2023) [29], who observed that ensemble-averaged maxima of O, H, OH, O(^{1}D), and O(^{1}S) in $NH_3/O_2/N_2$ mixtures under nanosecond plasma discharges exhibited a similar rise-and-fall trend as E/N increased, with radical concentrations peaking around 300 Td. The

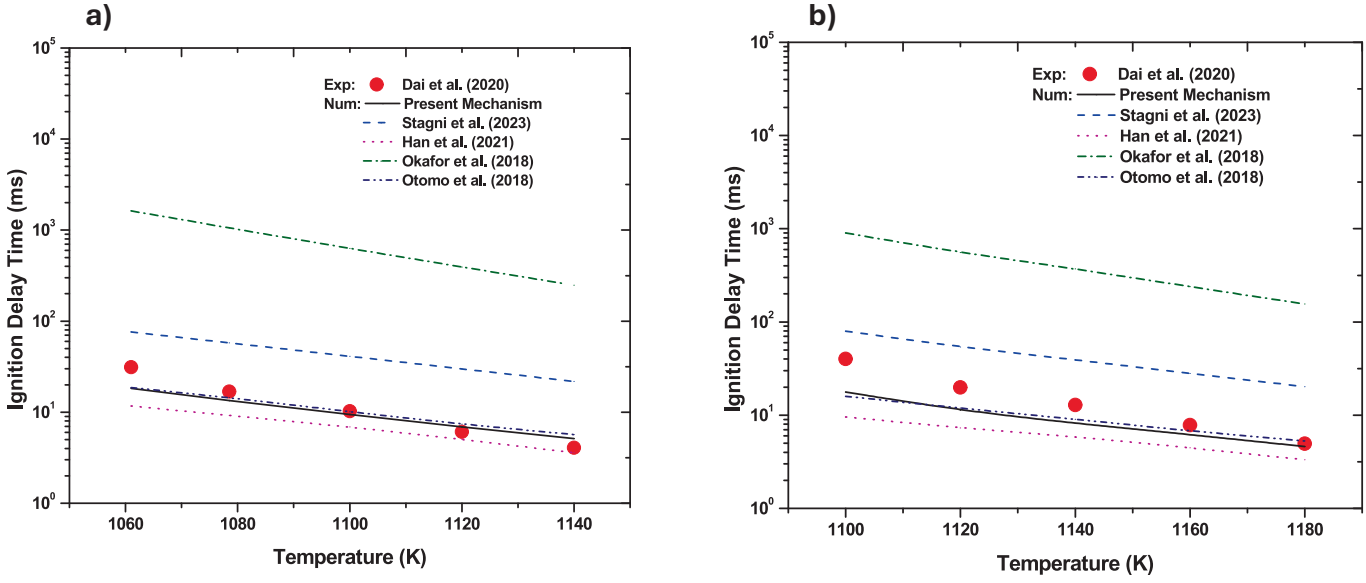


Fig. 2. IDTs of 0·.143NH_3/0.107O_2 /0.75Ar mixture as a function of temperature at a pressure of 60 bar, a) $\Phi = 0.5$ and b) $\phi = 1.0$. Symbols represent experimental data [12], while lines depict the simulated results from the present model and previous models [60–63].

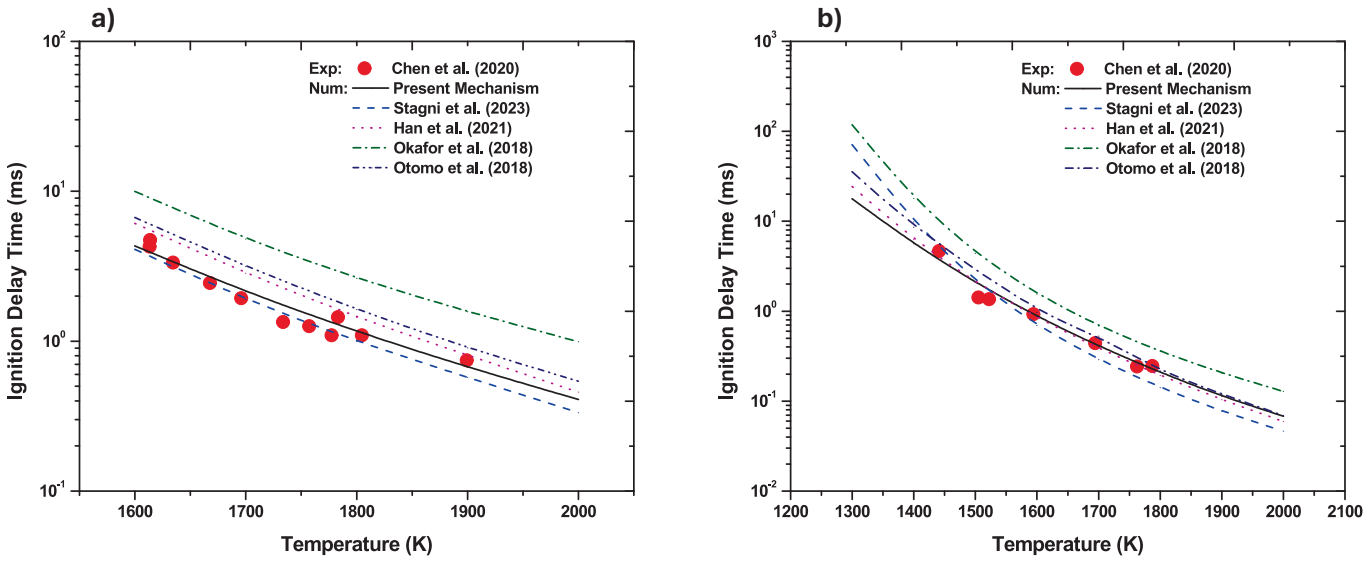


Fig. 3. IDTs of 0·.04375NH_3/0.03281O_2/0.92344 Ar mixture as a function of temperature at Φ = 1.0 and a pressure of a) 1.2 atm and b) 10 atm. Symbols represent experimental data [64], while lines depict the simulated results from the present model and previous models [60–63].

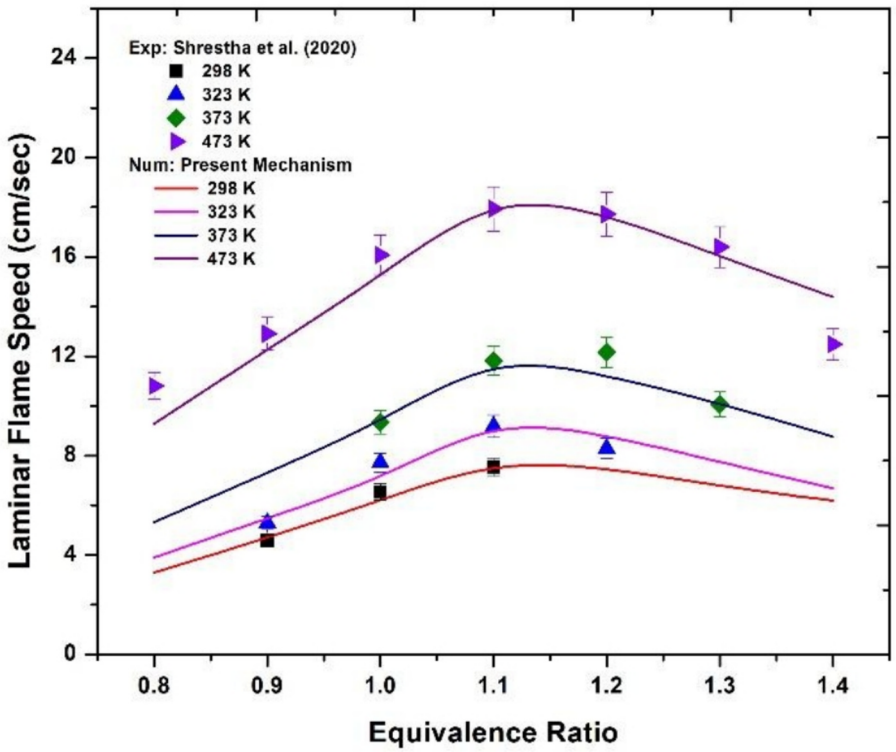


Fig. 4. LFS of NH_3/air flames at p = 1 atm and temperatures of 298 K, 323 K, 373 K, and 473 K. Symbols represent experimental data [65], while lines depict the simulated results from the present model.

authors attributed this behavior to the combined effects of radical recombination and precursor exhaustion, limiting net reactivity at high fields.

Furthermore, experimental and kinetic modeling work by Mao et al. (2024) [24] demonstrated that plasma-assisted ignition of NH_3/air mixtures exhibits a non-monotonic dependence on E/N, with an optimal value around 250 Td. Their study highlights that at high E/N, quenching of excited species such as N2*, O(^{1}D), and N(^{2}D) reduces the effectiveness of energy deposition, and that key OH-producing reactions (e.g., $NH_3 + OH \rightarrow NH_2 + H_2O$, $NH + O_2 \rightarrow NO + OH$) are critical for ignition, while others can inhibit radical propagation. These complementary results provide strong support for the interpretation proposed in the present work.

Hydrogen (H) and Oxygen (O) radicals are crucial in initiating chain reactions in combustion processes. Elevated production of H and O under higher E/N conditions can accelerate reaction rates and shorten ignition delay times (IDT). OH is a primary indicator of combustion efficiency and flame stability. Its initial rise and subsequent fall with increasing E/N highlight the delicate balance between production and recombination rates under plasma conditions. At high E/N values, OH

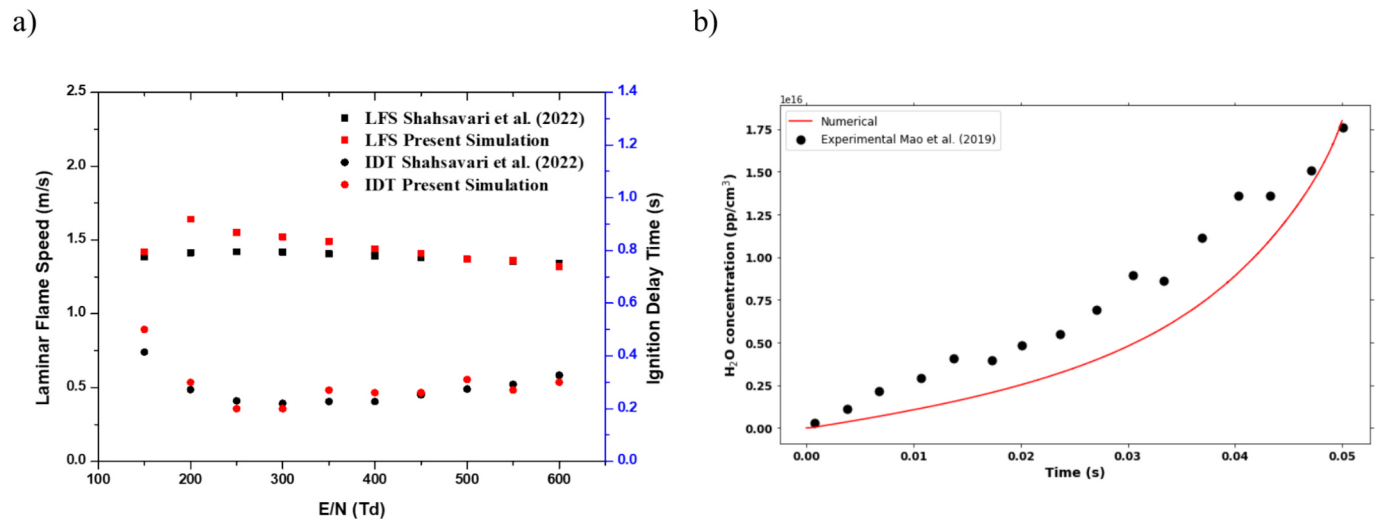


Fig. 5. A) plasma-assisted $nh_3/O_2/N_2$ combustion for $\phi = 1$, Tin = 850 K with PRF = 50 kHz and Ep = 5 mJ/cm^3 IDT and LFS. b) H_2O number density with model prediction during and after the 1500 pulse, 30 kHz nanosecond plasma in burst modes for a 0.1667 H_2/0.0833 O_2/0.75 He mixture at 60 Torr.

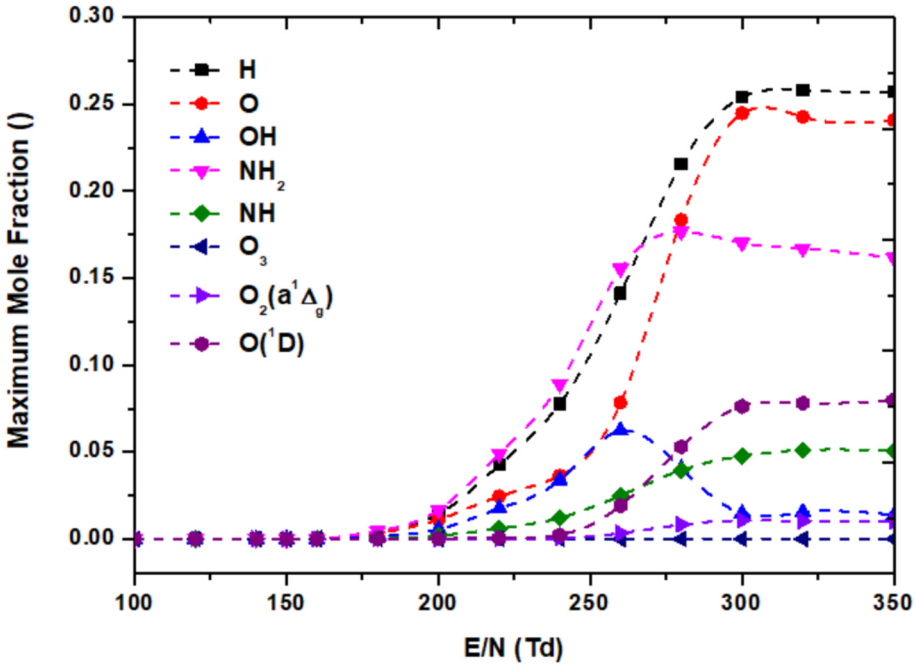


Fig.6. Maximum molar fractions of active and excited species in 20 pulses of NSPD in an NH_3/air mixture at T = 850 K, p = 1 atm, $\Phi = 1.0$ with PRF = 50 kHz.

depletion becomes significant due to secondary reaction pathways. As illustrated in Fig. 6, the OH mole fraction decreases with increasing E/N, as secondary reactions progressively consume OH and outweigh its primary plasma-driven production. The dominant OH-depleting reactions at elevated E/N include $O_2(a^1\Delta_g) + OH => O + HO_2$, $O(^1D) + OH => H + O_2$, and $N_2(A) + OH => N_2 + O + H$.

O_3 acts as a powerful oxidizer and contributes significantly to low-temperature reaction pathways. Its decline at higher E/N suggests that excessive electron energy might disrupt its stable formation pathways.

$O_2(a^1\Delta_g)$, a metastable electronically excited species, enhances oxidation pathways and flame propagation. Its linear increase across the E/N range indicates robust formation mechanisms under elevated E/N conditions.

NH_2 and NH are intermediates that are critical for fuel decomposition and NOx formation pathways. Their sustained increase with rising E/N suggests an enhanced ammonia decomposition process under plasma influence. Fig. 7 illustrates the influence of the reduced electric field (E/N) on the ignition delay time (IDT) for an NH_3/air mixture under the specified conditions. The results indicate that at low E/N values, the IDT remains relatively high, signifying slower ignition. However, as E/N increases to approximately 180 Td, the IDT decreases sharply, indicating enhanced ignition facilitation. As E/N increases to ~180 Td, the electron energy exceeds the thresholds for efficient dissociation of NH_3, N_2, and O_2, leading to a rapid increase in concentrations of radicals such as H, O, OH, NH, and NH_2, and excited species like O (^{1}D) and O_2 ($a^1\Delta_g$).

This transition effectively shifts the controlling mechanism from thermal ignition to plasma-enhanced chemical kinetics, causing a sharp reduction in IDT. Notably, this change is accompanied by multi-order of magnitude jumps in these species between 160 and 180 Td (e.g., H increases from $\sim 2.6 \times 10^{-5}$ to $\sim 3.9 \times 10^{-3}$, O rises from $\sim 2.5 \times 10^{-4}$ to $\sim 3.5 \times 10^{-3}$, and OH increases from $\sim 8.9 \times 10^{-5}$ to $\sim 1.5 \times 10^{-3}$). This

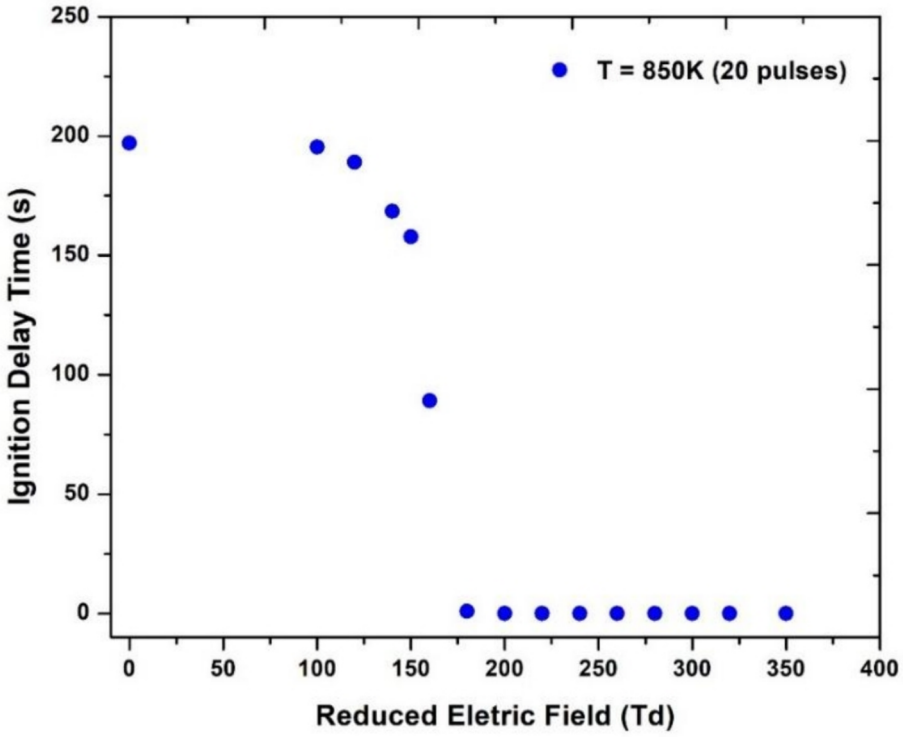


Fig. 7. Effect of E/N on IDT for an NH_3/air mixture at T = 850 K, p = 1 atm, and Φ = 1.0, with 20 pulses of NSPD at a PRF of 50 kHz.

shift enables rapid chain-branching reactions, causing the observed sharp drop in IDT.

Based on these findings, an E/N value of 180 Td is selected for subsequent investigations as it provides the most effective ignition enhancement.

While IDT reduction is a key indicator of ignition enhancement, other critical factors such as NOx emissions, flame stability, and system efficiency must also be considered. Future studies will assess the trade-offs between these factors to determine whether 180 Td remains the most practical choice for real-world plasma-assisted combustion applications.

To further validate this choice of 180 Td for simulation, the maximum reaction rate was evaluated across varying E/N levels, as presented in Figs. 8 and 9.

Fig. 8(a)–(d) and Fig. 8(a) and (b) show the maximum reaction rate for the key reactions contributing to the production of active and excited species over 20 plasma discharge pulses at various E/N values, under conditions of p = 1 atm, T = 850 K and PRF = 50 KHz. The data show that the maximum reaction rates increase as E/N rises from 140 Td to 220 Td. The results show that at 180 Td, a substantial quantity of active and excited species was produced.

H is primarily produced via NH_3 dissociation by electron impact and through reactions involving electronically excited oxygen species (O(^{1}D), O(^{1}S), O(A^1)), nitrogen states (N_2(^{1}A), N_2(AB)), and the ionized form NH_3^+, which absorbs electrons.

The primary reactions include:

- $E + NH_3 = E + NH_2^+$
- $E + NH_3 = E + NH + H + H$
- $NH_3^+ + E = NH_2 + H$
- $N_2(A) + H = N_2 + H$
- $N_2(AB) + H = N_2 + H$

O is produced through electron interactions with O_2, reactions involving electronically excited oxygen and nitrogen species, and reactions between O_3 and oxygen. The primary reactions responsible for generating O include: $E + O_2 = E + O + O$, $E + O_2 = E + O + O(^1D)$, $N_2(C) + O_2 = N_2 + O + O(^1S)$, $N_2(B) + O_2 = N_2 + O + O(^1D)$ and $O(^1D) + N_2 = O + N_2$.

Electron impact on oxygen molecules ($E + O_2 \rightarrow E + O + O$) remains a dominant pathway across all E/N values, while excited oxygen states (O(^{1}D), O(^{1}S), O_2 ($a^1\Delta_g$)) play a critical role in enhancing secondary reaction pathways.

Recombination and quenching reactions start dominating at higher E/N values (220 Td), reducing overall efficiency.

OH production is influenced by reactions involving electronically excited oxygen species (O(^{1}D), O(^{1}S), O_2 ($a^1\Delta_g$)) and nitrogen species (N_2(A)).

The primary reactions for producing OH include $O(^1D) + NH_3 = OH + NH_2$, $O(^1D) + H_2O = OH + OH$, $O(^1S) + H_2O = OH + OH$, O_2 ($a^1\Delta_g$) + $H = OH + O$, and $N_2(A) + H_2O = N_2 + H + OH$.

The pathway $O(^1D) + NH_3 = OH + NH_2$, $O(^1D) + H_2O = OH + OH$ shows consistent high reaction rates across E/N values, with a peak observed around 180 Td.

At higher E/N values (220 Td), recombination and competing pathways reduce OH production efficiency.

NH_2 shows a consistent increase in reaction rates with rising E/N values (140 Td → 220 Td).

The production of NH_2 and NH is driven by the reactions involving electrons and electronically excited N_2(A) and O(^{1}D).

The production rate of NH_2 peaks for key pathways such as $E + NH_3 = E + NH_2 + H$ and $O(^1D) + NH_3 = OH + NH_2$.

The key NH formation reactions from the figure highlight multiple pathways contributing to the production of NH radicals under varying E/N values. The reaction $E + NH_3 \rightarrow E + NH_2 + H$ represents electron-impact dissociation of ammonia, producing NH_2 and H. Its reaction rate shows a significant increase as E/N rises from 140 Td to 220 Td, indicating enhanced electron energy transfer facilitating NH_2 formation, which acts as an intermediate for NH production. Another significant pathway is $E + NH_3 \rightarrow E + NH + H + H$, where NH_3 dissociates directly into NH and two H radicals under electron impact. This reaction steadily increases in rate across the E/N range, reflecting its growing dominance

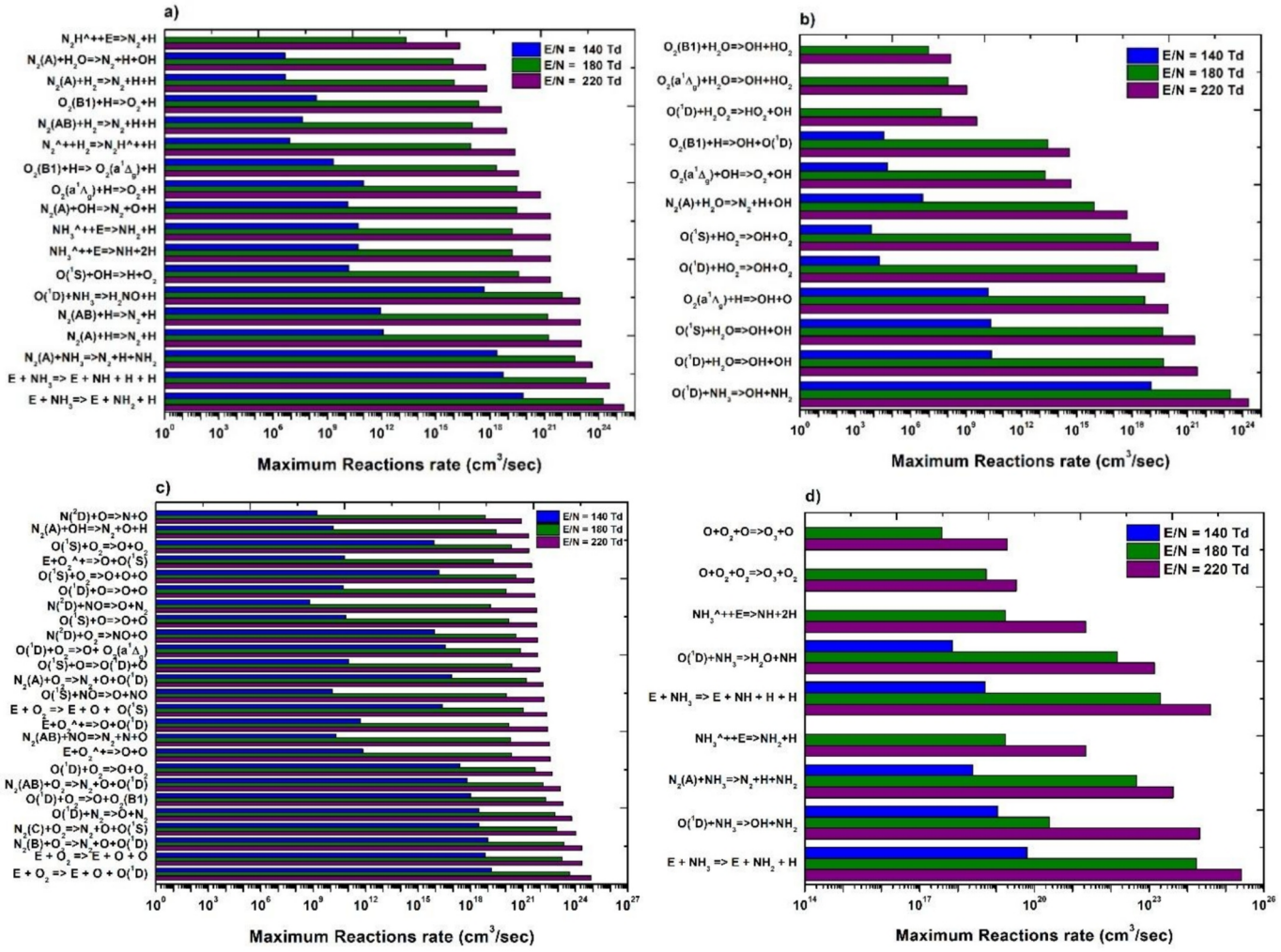


Fig. 8. The maximum reaction rate for the important reactions that participate in the production of a) H. b) OH. c) O, and d) NH_2, NH, O_3 during 20 pulses of NSPD at p = 1 atm, T = 850 K, and PRF = 50 kHz.

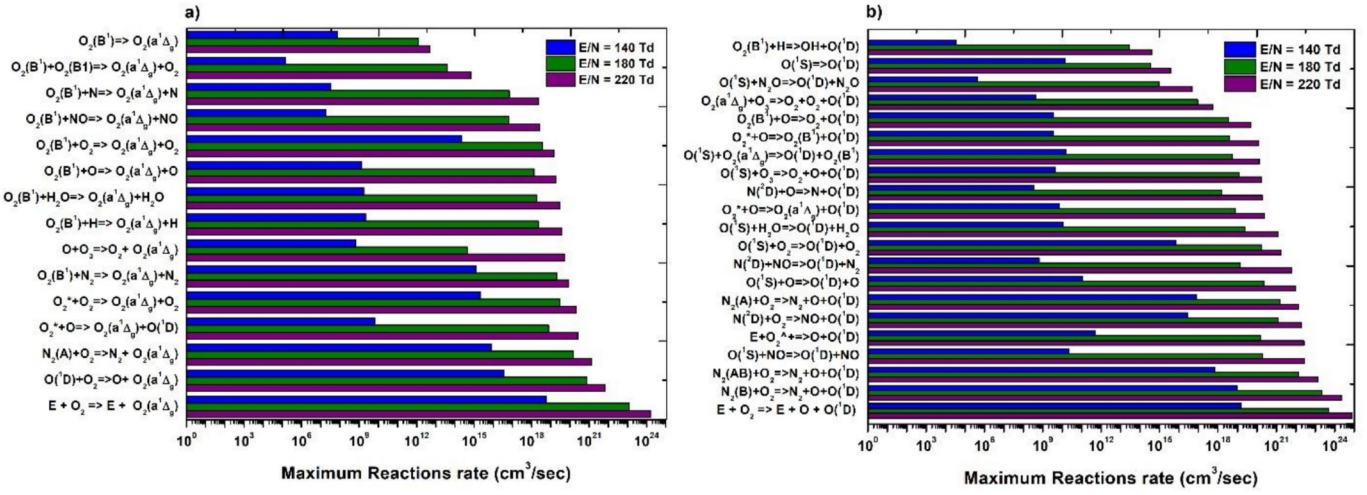


Fig. 9. The maximum reaction rate for the important reactions that participate in the production of a) O_2 ($a^1\Delta_g$) and b) $O(^1D)$ during 20 pulses of NSPD at p = 1 atm, T = 850 K, and PRF = 50 kHz.

at higher reduced electric fields.

Additionally, the reaction $O(^1D) + NH_3 \rightarrow NH + OH + H$ plays a vital role in NH formation, with electronically excited oxygen species interacting with NH_{33} to produce NH, OH, and H. Its reaction rate significantly increases at E/N = 180 Td and continues rising at 220 Td, underscoring the importance of excited oxygen species in enhancing NH

production. Similarly, the reaction $N_2(A) + NH_2 \rightarrow N_2 + NH + H$, involving electronically excited nitrogen ($N_2(A)$) interacting with NH_2 radicals, contributes to NH formation. The rate of this reaction steadily increases with E/N, highlighting the role of excited nitrogen in the decomposition of ammonia-derived intermediates.

Lastly, the reaction $NH_3^+ + E \rightarrow NH + H + H$ represents the recombination of NH_3^+ ions with electrons, leading to NH and two H radicals. While this reaction shows an increase in rate with rising E/N, it appears to plateau at 220 Td, suggesting potential energy saturation effects at higher electric fields. These reactions collectively emphasize the interplay between electron-impact dissociation, excited species interactions, and ion recombination processes in determining NH yields across different E/N values.

From Fig. 9, it is evident that $O_2(a^1\Delta_g)$ formation increases consistently with rising E/N, highlighting the critical role of electron energy in promoting the excitation of molecular oxygen.

At lower E/N values (140 Td), the production of $O_2(a^1\Delta_g)$ is primarily driven by direct electron-impact excitation reactions such as $E + O_2 \rightarrow E + O_2(a^1\Delta_g)$ and secondary pathways involving collisions with electronically excited nitrogen species like $N_2(A) + O_2 \rightarrow N_2 + O_2(a^1\Delta_g)$. These reactions demonstrate moderate reaction rates, suggesting that electron energy at 140 Td is sufficient to trigger initial excitation processes but remains limited in sustaining higher yields of $O_2(a^1\Delta_g)$.

As E/N increases to 180 Td, a substantial enhancement in $O_2(a^1\Delta_g)$ production is observed. This can be attributed to more efficient electron energy transfer during collisions, which amplifies the yield of electronically excited oxygen species. Additionally, reactions involving metastable species such as $O(^1D) + O_2 \rightarrow O + O_2(a^1\Delta_g)$ and $O_2(B^1) + O \rightarrow O_2(a^1\Delta_g) + O$ become increasingly significant contributors to $O_2(a^1\Delta_g)$ formation at this intermediate E/N range. This indicates that both direct electron-impact excitation and secondary reaction pathways are optimized at 180 Td, resulting in peak production rates.

At 220 Td, the production of $O_2(a^1\Delta_g)$ continues to increase, albeit at a slower rate. This plateau effect suggests that competing pathways, such as quenching and recombination reactions, start to counterbalance the enhanced excitation effects. For instance, reactions like $O_2(a^1\Delta_g) + O \rightarrow O_2 + O(^1D)$ and other energy-dissipating processes might reduce the net formation of $O_2(a^1\Delta_g)$.

Overall, the trends suggest that $O_2(a^1\Delta_g)$ production benefits most from intermediate E/N values (around 180 Td), where electron impact and secondary excitation pathways are balanced effectively. Beyond this range, competing reactions and energy saturation effects hinder further efficiency gains. Understanding these dynamics is crucial, as $O_2(a^1\Delta_g)$ plays a pivotal role in enhancing flame propagation and influencing low-temperature oxidation pathways in plasma-assisted combustion systems.

The formation of the excited oxygen state $O(^1D)$ is primarily depicted in the right-hand plot (b), highlighting key reaction pathways contributing to its production. The results indicate that the formation of $O(^1D)$ occurs predominantly through dissociation and excitation processes involving molecular oxygen O_2 and nitrogen N_2, as well as via collisions with electronically excited species.

In particular, the reaction pathways such as $E + O_2 = E + O + O(^1D)$ underscore the importance of electron impact dissociation, where high-energy electrons collide with molecular oxygen, breaking its bonds and yielding the excited $O(^1D)$ state. This pathway is highly dependent on the reduced electric field (E/N) and the electron energy distribution, with higher electric fields favoring more frequent and energetic collisions.

Another critical pathway, $N_2(B) + O_2 = N_2 + O + O(^1D)$, highlights the contribution of excited nitrogen molecules $N_2(B)$ in transferring energy to oxygen molecules, leading to dissociation and the formation of $O(^1D)$. Similarly, the reaction $N_2(AB) + O_2 = N_2 + O + O(^1D)$ suggests that both vibrational and electronic excitation states of nitrogen molecules can play a role in enhancing the dissociation efficiency of oxygen. The pathway $O(^1S) + NO = O(^1D) + NO$ reveals the importance of interspecies energy transfer, where an electronically excited oxygen atom $O(^1S)$ collides with nitric oxide (NO), transferring energy and decaying to the $O(^1D)$ state. This process demonstrates the interplay between reactive intermediates in plasma environments.

Lastly, the reaction $E + O_2^{\wedge+} = O + O(^1D)$ emphasizes the role of ionic species in generating excited oxygen states. Here, electron collisions with molecular oxygen ions $O_2^{\wedge+}$ facilitate dissociation into neutral oxygen atoms, including the highly reactive $O(^1D)$.

3.2. Effect of plasma discharge and initial temperature on IDT

Fig. 10 illustrates the impact of initial temperature and NSPD, with 20 pulses, on the NH_3/air mixture at a constant E/N of 180 Td within the intermediate temperature range of 850 K to 1100 K on IDT, at atmospheric pressure, an equivalence ratio $\Phi = 1.0$, and a pulse repetition frequency (PRF) of 50 kHz.

The results indicate that the IDT in plasma-assisted cases is significantly shorter compared to cases without plasma. This improvement is primarily due to the plasma producing reactive radicals (e.g., H, O, OH) and excited species (e.g., O_2 ($a^1\Delta_g$), $O(^1D)$), which accelerate reaction rates and introduce new reaction pathways. Specifically, the IDT decreased from 197.377 s to 1.614 s with 20 pulses of NSPD at an initial temperature of 850 K.

The results further indicate that increasing the initial temperature of the mixture from 850 K to 1100 K leads to a decrease in the IDTs in both plasma-assisted and non-plasma cases. Without plasma, raising the initial temperature from 850 K to 1100 K significantly reduces the IDT from 197.377 s to 0.356 s. In plasma-assisted cases, as the initial temperature rises from 850 K to 1100 K, the IDT decreases from 1.614 s to 0.027 s with 20 pulses of NSPD.

In the plasma cases, it is observed that the reduction in IDT is more pronounced at lower initial temperatures across all cases, highlighting a stronger impact of plasma under these conditions. Specifically, at an initial temperature of 850 K, the IDT decreased significantly from 197.377 s to 1.614 s, whereas at 1100 K, it dropped from 0.356 s to 0.027 s with 20 pulses. As the temperature of the mixture increases, the production of active and excited species (H, OH, O, NH_2, NH, O_3, O_2 ($a^1\Delta_g$), and $O(^1D)$) during the plasma discharge decreases, as shown in Fig. 11, thereby diminishing the plasma's influence at higher temperatures.

3.3. IDT sensitivity analysis

To analyze the impact of plasma on IDT, a reaction sensitivity

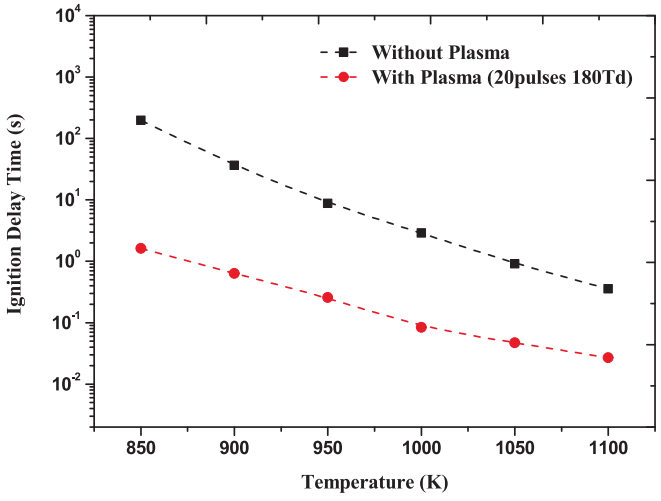


Fig. 10. IDT without and with 20 pulses of NSPD in NH_3/air mixture at p = 1 atm, $\Phi = 1.0$, E/N = 180 Td, and a PRF of 50 kHz.

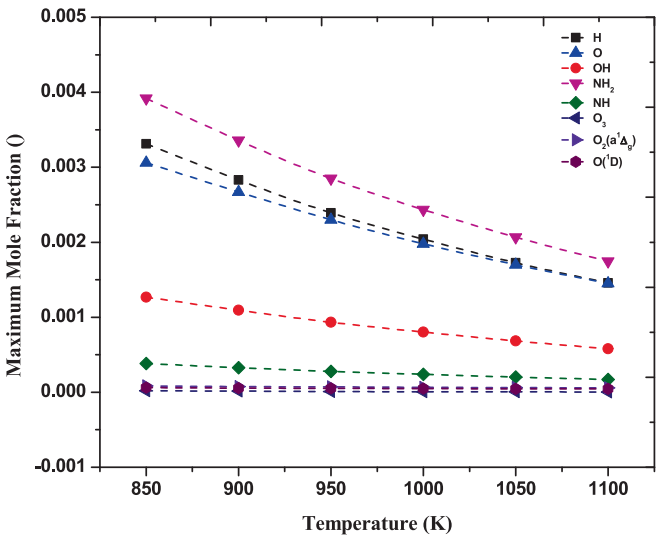


Fig. 11. Production of active and excited species during the 20 pulses of NSPD in NH_3/air mixture at p = 1 atm, Φ = 1.0, E/N = 180 Td, and a PRF of 50 kHz.

analysis was conducted both without and with 20 pulses of NSPD at initial temperatures of 850 K and 1050 K, under conditions p = 1 atm, E/N = 180Td, and PRF = 50KHz, as shown in Fig. 12. The brute-force sensitivity of the IDT to a given reaction was assessed by doubling the pre-exponential factor of the rate constant and calculating the relative change in IDT. Reactions with positive sensitivity values tend to inhibit ignition by increasing the IDT, whereas those with negative sensitivities promote ignition by reducing the IDT.

Fig. 12 presents the sensitivity analysis of temperature variations on IDT at 850 K and 1050 K. By comparing the relative impact of plasma at 850 K and 1050 K, the analysis confirms that plasma-induced kinetic enhancements are more pronounced at lower temperatures, where thermal reaction rates are slower. This demonstrates that the reduced benefit of plasma at higher temperatures is not due to a drop in radical production, but rather to the diminishing marginal effect of plasma on already fast thermal chemistry.

Reactions involving NH_2 and N_2H_x species significantly influence IDT outcomes, with the reaction $NH_2 + NO <=> NNH + OH$ identified as the most impactful reaction for improving IDT. Under plasma conditions, this reaction's normalized brute-force sensitivity increases by 9 %. The reactions $H_2NO + O_2 <=> HNO + HO_2$ and $HO_2 + NH_2 <=> H_2NO + OH$ become 2 to 3 times more impactful on the IDT with the introduction of plasma. Additionally, reactions, where the H atom participates as a reactant, show an impact that is three times greater. Among the reactions that inhibit the ignition delay time, the reaction $NH_2 + NO <=> H_2O + N_2$ competes with $NH_2 + NO <=> NNH + OH$, as detailed in [12]. The presence of plasma increases the sensitivity of this reaction by 8 %. Conversely, the reaction $NH_2 + NO_2 <=> H_2O + N_2O$ is 20 % less inhibiting, while $H_2NO + NH_2 <=> HNO + NH_3$ and $H_2NO + HO_2 <=> H_2O_2 + HNO$ have a threefold reduction in impact.

At 1050 K, the competitive NH_2 reactions are the most influential in either promoting or inhibiting IDT. The main difference compared to the 850 K case is that the plasma effect enhances the reaction $NH_2 + NO <=> NNH + OH$ by only 2 %, while the inhibiting effect of the reaction $NH_2 + NO <=> H_2O + N_2$ decreases by 5 %, contrary to the increase observed at 850 K. Among the most important reactions, it is again noted that reactions involving H as a reactant become significantly more critical when the plasma effect is active.

Specifically, the reaction $H + O_2 <=> O + OH$ becomes the second least sensitive reaction with brute-force sensitivity reduced by 2.7 times compared to the non-plasma case. In contrast, the reactions $H_2NO + O_2 <=> HNO + HO_2$ and $NH_2 + NO_2 <=> H_2O + N_2O$ show a strong reduction in their impact on IDT, as plasma significantly reduces its influence. However, this effect is not seen in other reactions, where plasma either consistently enhances or has a negligible influence on the reactions' impact on IDT.

3.4. Effect of plasma and equivalence ratio on LFS

The LFS is a crucial combustion parameter that indicates the rate at which a flame front propagates through an unburned fuel mixture. Ammonia is known for its relatively low flame speed compared to hydrogen and hydrocarbon fuels, underscoring a better understanding of the impact of plasma on NH_3/air flame speed to optimize NH_3 combustion processes. Tables 3, 4 and 5 present the concentrations of active and excited species produced during the 20 pulses of NSPD at initial temperatures of 350 K, 450 K, and 550 K across various equivalence ratios, which are used as input for the LFS combustion simulations.

Fig. 13 shows the effect of initial temperatures, Φ, and 20 pulses of NSPD on the LFS of ammonia/air mixture under conditions of 1 atm, E/N = 180Td, and PRF = 50KHz. The results show that increasing the initial temperature of the mixture leads to higher LFS. This is because high temperatures provide additional energy, which promotes chemical reactions and accelerates flame propagation. This trend is consistent across both plasma-assisted and non-plasma cases, with the highest LFS

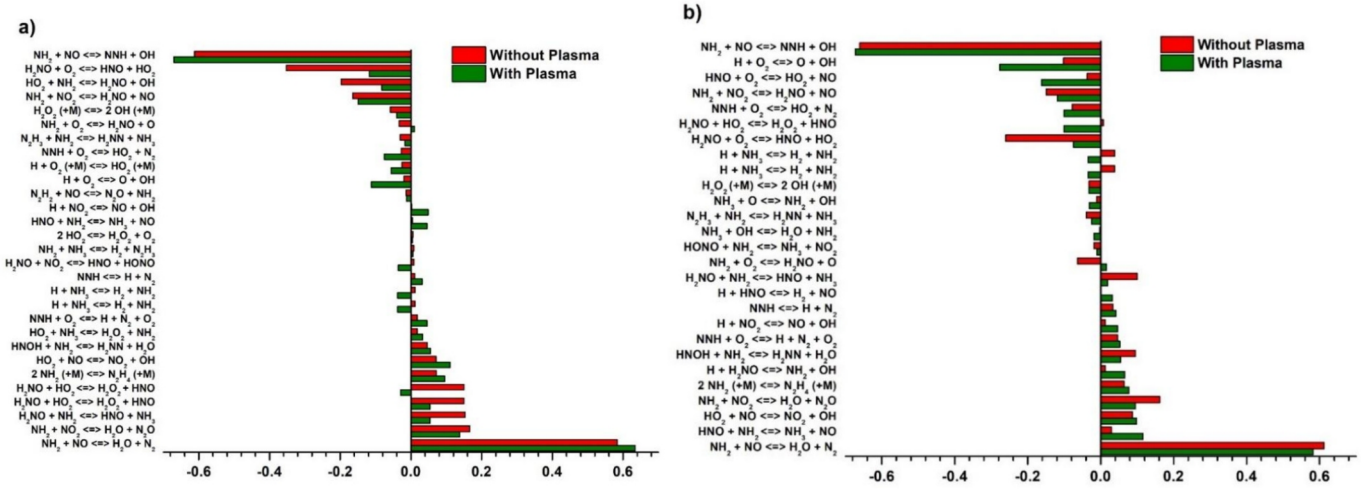


Fig. 12. IDT Sensitivity analysis for NH_3/air mixture without and with 20 pulses of NSPD at p = 1 atm, Φ = 1, E/N = 180Td, and PRF = 50KHz. a) 850 K and b) 1050 K.

Table 3
Maximum molar fractions of active and excited species at different equivalence ratios during 20 pulses of NDPD at p = 1 atm, T = 350 K, E/N = 180Td, and PRF = 50KHz.

Equivalence ratio	H	O	OH	NH_2	NH	O_3	O_2 ($a^1\Delta_g$)	O(^{1}D)
0.7	0.01738	0.00674	0.00751	0.02136	0.00202	0.00647	1.6989E-4	2.912E-4
0.8	0.02182	0.0073	0.00884	0.0262	0.00252	0.00664	0.000205	0.000325
0.9	0.02697	0.00786	0.01026	0.03168	0.0031	0.00674	0.000213	0.000356
1.0	0.03216	0.00843	0.01149	0.03702	0.00368	0.00681	0.000213	0.000391
1.1	0.03778	0.00896	0.01275	0.04273	0.0043	0.00676	0.000215	0.000439
1.2	0.04398	0.00945	0.01404	0.04894	0.00498	0.00671	0.000259	0.00048
1.3	0.05007	0.0099	0.01517	0.05489	0.00564	0.00668	0.000294	0.000532
1.4	0.05699	0.01043	0.01645	0.06165	0.00638	0.00662	0.000299	0.000562

Table 4
Maximum molar fractions of active and excited species at different equivalence ratios during 20 pulses of NSPD at p = 1 atm, T = 450 K, E/N = 180Td, and PRF = 50KHz.

Equivalence ratio	H	O	OH	NH_2	NH	O_3	O_2 ($a^1\Delta_g$)	O(^{1}D)
0.7	0.00909	0.00652	0.00399	0.01124	0.00106	0.00137	1.652E-4	1.5368E-4
0.8	0.01137	0.00699	0.00467	0.01372	0.00131	0.00139	0.000017	0.000166
0.9	0.01385	0.00736	0.00533	0.01635	0.00159	0.00142	0.000178	0.000177
1.0	0.01671	0.00782	0.00604	0.01933	0.00191	0.00141	0.000176	0.00019
1.1	0.01957	0.00814	0.00667	0.02224	0.00222	0.00142	0.00018	0.000203
1.2	0.02283	0.00853	0.00735	0.0255	0.00257	0.00141	0.000193	0.000203
1.3	0.02609	0.00883	0.00796	0.0287	0.00292	0.0014	0.00012	0.000226
1.4	0.02943	0.00913	0.00853	0.03194	0.00328	0.00137	0.000198	0.000238

Table 5
Maximum molar fractions of active and excited species at different equivalence ratios during 20 pulses of NSPD at p = 1 atm, T = 550 K, E/N = 180Td, and PRF = 50KHz.

Equivalence ratio	H	O	OH	NH_2	NH	O_3	O_2 ($a^1\Delta_g$)	O(^{1}D)
0.7	0.00551	0.00559	0.00243	0.00683	6.40663E-4	3.32953E-4	1.5007E-4	1.0406E-4
0.8	0.00683	0.00597	0.00282	0.00827	0.00079	0.000341	0.00149	0.000111
0.9	0.00834	0.00639	0.00323	0.00988	0.00096	0.000346	0.000152	0.000116
1.0	0.00993	0.0067	0.00361	0.01153	0.00113	0.000351	0.000157	0.000121
1.1	0.01164	0.00705	0.00399	0.01327	0.00132	0.000352	0.000153	0.000126
1.2	0.01355	0.00739	0.00439	0.01518	0.00153	0.000354	0.000155	0.000133
1.3	0.0155	0.00769	0.00475	0.01711	0.00173	0.000351	0.000151	0.000137
1.4	0.01753	0.00798	0.0051	0.01908	0.00195	0.000348	0.000153	0.000143

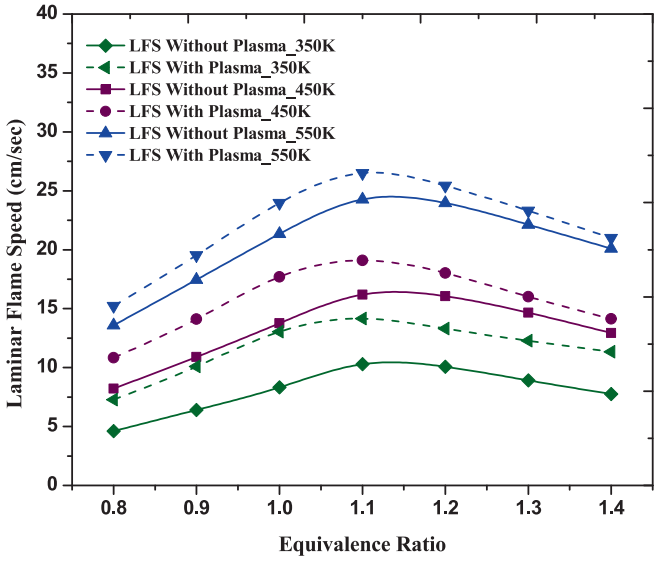


Fig. 13. LFS of NH_3/air flames at different equivalence ratios without and with 20 pulses of NSPD at p = 1 atm, E/N = 180 Td, PRF = 50KHz, and different initial temperatures.

values observed at $\Phi \approx 1.1$. Specifically, the LFS increases from 10.29 cms^{-1} to 26.5 cm^{-1} without plasma and from 14.15 cms^{-1} to 26.5 cms^{-1} with plasma as the initial temperature increases from 350 K to 550 K at $\Phi = 1.1$ and 1 atm.

The results also demonstrated that plasma significantly enhances the LFS. Specifically, the plasma increases LFS from 10.29 cms^{-1} to 14.15 cms^{-1} (37.5 %), from 16.19 cms^{-1} to 19.1 cms^{-1} (18 %), and from 24.28 cms^{-1} to 26.5 cms^{-1} (9.1 %) at $\Phi = 1.1$, p = 1 atm, and initial temperatures of 350 K, 450 K, and 550 K, respectively. The enhancement in flame speed is most pronounced at the lower initial temperature of 350 K, where plasma generates higher concentrations of active radicals and excited species, which accelerate key reaction pathways and enable faster combustion.

As observed in Tables 3, 4 and 5, the peak molar fractions of key species such as H, O, OH, NH_2, and O(^{1}D) are significantly higher at 350 K compared to 450 K and 550 K. At $\Phi = 1.1$, the molar fraction of H decreases from 0.03778 at 350 K to 0.01957 at 450 K (48.2 %) and further decreases to 0.01164 at 550 K (69.2 %). Similarly, OH drops from 0.01275 to 0.00667 (47.7 %) and then to 0.00399 (68.7 %), while NH_2 declines from 0.04273 to 0.02224 (47.9 %) and to 0.01327 (68.9 %) as the temperature increases from 350 K to 450 K and 550 K, respectively. Other species, including O(^{1}D), O, and NH, follow the same trend; for example, O(^{1}D) decreases by 53.7 % at 450 K and 71.3 % at 550 K relative to 350 K. These consistent reductions indicate that plasma's contribution is most effective at lower temperatures, where the enhanced production of reactive intermediates plays a dominant role in

accelerating flame propagation.

3.5. LFS sensitivity analysis

To identify the key reactions affecting the LFS of NH_3/air mixtures, a reaction sensitivity analysis was conducted both without and with 20 pulses of NSPD at various equivalence ratios, under conditions T = 450 K, p = 1 atm, E/N = 180Td, and PRF = 50KHz, as shown in Fig. 14.

In Fig. 14, positive sensitivity indicates that a reaction enhances reactivity (increasing LFS), while negative sensitivity shows that the reaction hinders reactivity. Across all conditions, with and without plasma, the chain-branching reaction $O_2 + H = OH + O$ is the most influential reaction for ammonia combustion, with its sensitivity further amplified by plasma, contributing to the accelerated laminar flame speed. Other highly sensitive reactions include the NNH radical, a key intermediate in NH_3 oxidation. The thermal dissociation reaction $NNH = N_2 + H$ increases reactivity by producing additional reactive H-atoms, whereas the oxidation reaction $NNH + O_2 = N_2 + HO_2$ decreases reactivity by producing less reactive HO_2 radicals.

However, when comparing across the equivalence ratios, it is evident that plasma-induced enhancements are more pronounced at lean conditions (Φ = 0.8). In this regime, the green bars (with plasma) are visibly longer than the red ones (without plasma), indicating a stronger plasma effect in promoting or inhibiting specific reactions. Conversely, at stoichiometric (Φ = 1.0) and rich (Φ = 1.2) conditions, the differences between plasma and non-plasma sensitivities are significantly reduced, and in some cases nearly overlap.

This progressive reduction in plasma effect with increasing equivalence ratio suggests that under stoichiometric and fuel-rich conditions, the thermal contribution to radical formation is already substantial, thereby diminishing the relative impact of non-thermal plasma. The similar bar heights at Φ = 1.0 and Φ = 1.2 for key reactions such as $H + O_2 \rightleftharpoons O + OH$ and $NH_2 + NO \rightleftharpoons NNH + OH$ confirm this behavior. Additionally, negative sensitivities, especially those involving $NNH + O_2 \rightleftharpoons HO_2 + N_2$, become less severe under plasma conditions, particularly at lean Φ, contributing to improved LFS.

3.6. The effect of plasma on the gas temperature and mole fraction profiles of NH_3/air

To better understand how plasma influences the LFS of ammonia/air mixture, gas temperature, and radical mole fraction analyses were performed. Fig. 15 presents the simulated gas temperature and mole fraction profiles for key radicals (H, O, HO, NH_2, and NH), which play essential roles in controlling flame speed and defining the primary reaction zone.

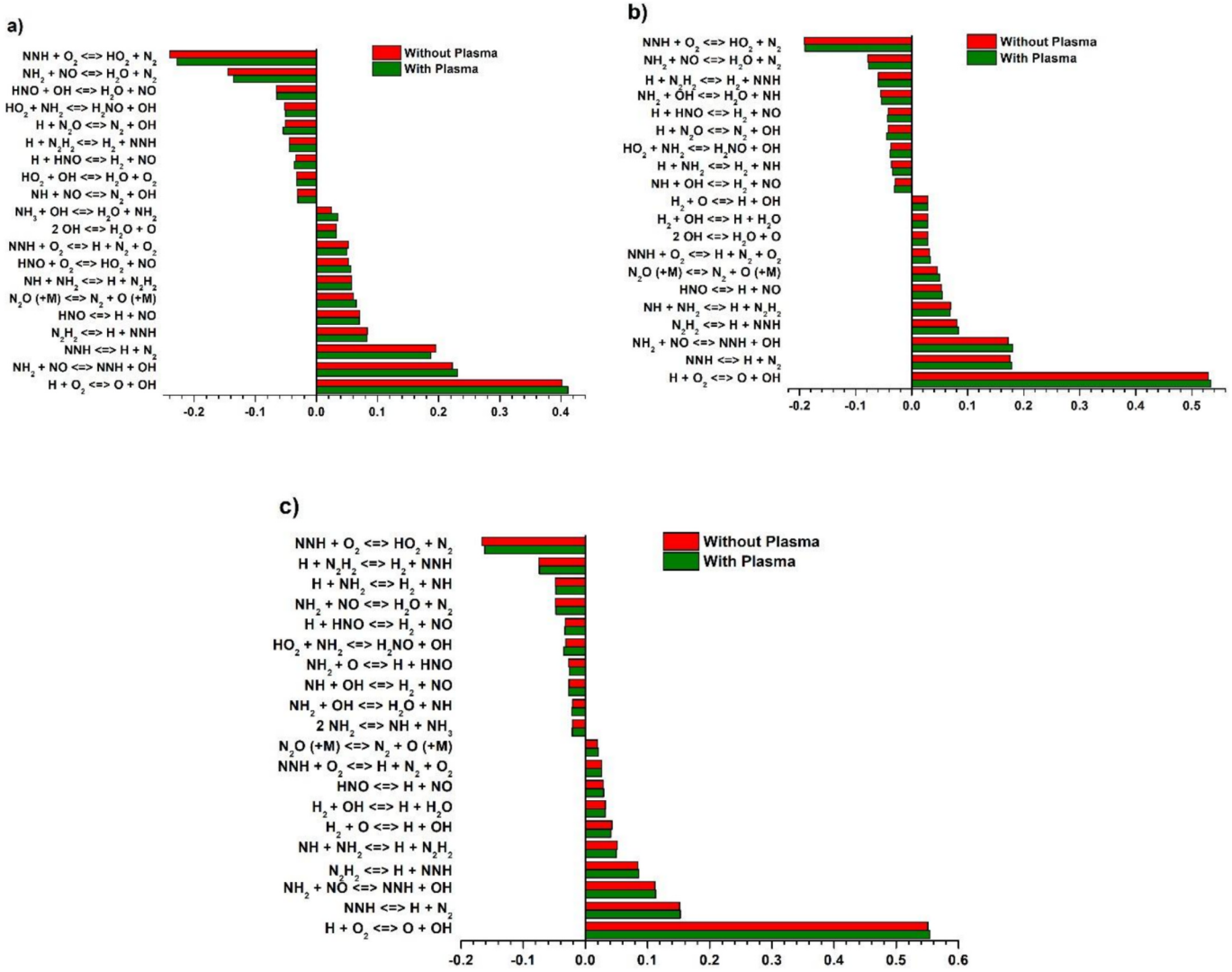


Fig. 14. Sensitivity analysis for LFS of NH_3/air without and with 20 pulses of NSPD at T = 450 K, p = 1 atm, E/N = 180Td, and PRF = 50KHz. a) Φ = 0.8. b) Φ = 1.0 and c) Φ = 1.2.

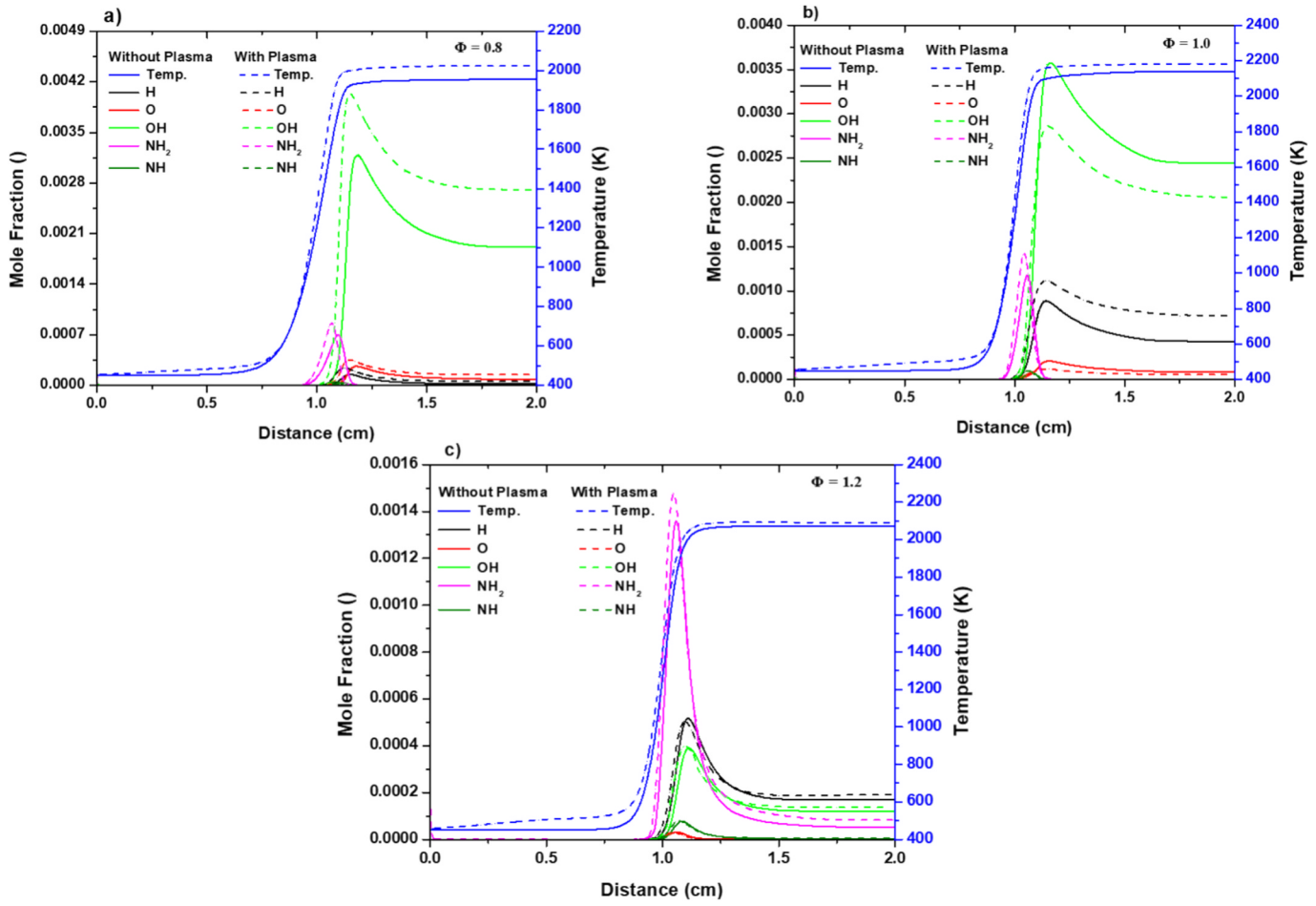


Fig. 15. Gas temperature and radical mole fraction profile for the ammonia/air mixture without and with 20 pulses of NSPD at T = 450 K, p = 1 atm, E/N = 180Td, and PRF = 50 kHz. a) Φ = 0.8. b) Φ = 1.0 and c) Φ = 1.2.

The results show that plasma application increases both the gas temperature and the mole fraction of all key reactive species. The total energy deposited via nanosecond pulsed discharges is relatively low and insufficient to account for a significant bulk gas heating via Joule (ohmic) effects alone. Furthermore, the final gas temperature increases by less than 2 % under plasma activation, which is within the expected variation range due to minor shifts in the reaction pathway and heat release distribution.

This slight increase is not attributed to direct thermal input from the plasma, but rather to kinetic enhancement; the presence of highly reactive radicals (H, O, OH), generated via electron impact dissociation and relaxation of excited species, shortens the ignition delay and anticipates the onset of exothermic reactions.

Among these, $O(^1D)$ reacts with key fuel and product species through reactions such as $O(^1D) + NH_3 \rightarrow OH + NH_2$; $O(^1D) + H_2O \rightarrow OH + OH$; $O(^1D) + H_2 \rightarrow OH + H$. These exothermic reactions release chemical energy rapidly and locally, contributing to an advanced onset of thermal rise and radical buildup.

Notably, peaks for reactive radicals such as OH, H, and O are much higher in the plasma-assisted cases under lean and stoichiometric conditions, while the effect is minimal under rich conditions. These peaks represent the primary reaction zone, where intense chemical reactions occur as ammonia decomposes and reacts with oxygen. This peak signifies the area within the reactor where the fuel mixture reaches optimal conditions for radical generation, breaking down ammonia and forming intermediate species that drive combustion. Plasma assistance amplifies this process, promoting the formation of reactive radicals even at lower initial temperatures. As a result, the plasma-assisted case shows elevated mole fractions of key radicals (visible in the dashed lines) compared to the non-plasma case. The enhanced radical concentrations contribute to faster and more efficient combustion, accelerating flame propagation and stabilizing the flame. As the reaction progresses beyond this zone, the concentrations of radicals gradually decline as they are consumed, giving way to the formation of stable combustion products like N_2 and H_2O. This decay in radical concentration marks the transition from the highly reactive phase to a more stable combustion phase, demonstrating how plasma enhances reactivity and flame stability within the ammonia-air mixture.

Overall, plasma significantly increases flame temperature and accelerates the accumulation of reactive species such as H, O, OH, NH_2, and NH, which boost reaction kinetics, enhance combustion efficiency, and increase flame speed.

4. Conclusion

The results show that increasing the reduced electric field (E/N) from 100 Td to 350 Td boosts the production of reactive species such as H, O, NH_2, NH, O_2 ($a^1\Delta_g$), and $O(^1D)$. In contrast, species like OH and O_3 show an initial rise from 100 Td to 280 Td, followed by a gradual decline due to recombination reactions.

In plasma-assisted ammonia combustion, the IDT is significantly reduced compared to non-plasma conditions. This suggests that plasma excitation accelerates reactions and introduces new pathways, enhancing NH_3 ignition at lower temperatures. The reduction in IDT is more pronounced at lower temperatures across all cases, suggesting that the impact of plasma on IDT is more pronounced at lower initial

temperatures. As the temperature of the mixture increases, the production of active and excited species during the plasma discharge decreases, thereby diminishing the plasma's influence at higher temperatures.

The sensitivity analysis for IDT shows that plasma significantly enhances the sensitivity of key reactions, particularly those involving NH_2 and H atoms as reactants, thereby accelerating ignition. Among these, the reaction $NH_2 + NO <=> NNH + OH$ is identified as the most impactful reaction for improving ignition delay time.

The results demonstrated that plasma significantly enhances the LFS compared to non-plasma scenarios, with the highest LFS observed at an equivalence ratio of $\Phi \approx 1.1$. Specifically, LFS increases from 10.29 cms^{-1} to 14.15 cms^{-1}, from 16.19 cms^{-1} to 19.1 cms^{-1}, and from 24.28 cms^{-1} to 26.5 cms^{-1} at $\Phi = 1.1$, p = 1 atm, and initial temperatures of 350 K, 450 K, and 550 K without and with plasma, respectively. It is also observed that at a low initial temperature of 350 K, the improvement in the flame speed is higher as compared to higher temperature conditions because plasma generates higher concentrations of active radicals and excited species at low temperatures. These radicals enhance key reaction pathways, facilitating faster combustion.

The sensitivity analysis for LFS reveals that the chain-branching reaction $O_2 + H = OH + O$ is the most sensitive reaction for ammonia combustion, with its sensitivity further amplified by plasma, explaining the acceleration in LFS.

While the proposed plasma-assisted model can be reasonably extrapolated to elevated pressures based on the validated high-pressure chemical kinetics, it should be noted that increased pressure may affect electron kinetics, vibrational excitation, and radical formation pathways, potentially modifying the ignition enhancement observed at ambient pressure; therefore, future high-pressure plasma-assisted experiments will be essential for rigorous validation.

Declaration of competing interest

None.

Acknowledgment

This work was supported by the project Intermingle: Mild-Oxidation and Plasma Roadmaps for Hydrogen/Ammonia Energy Vectors (Project ID: P20229WXJP_001), funded under the PRIN PNRR 2022 call by the European Union – NextGenerationEU, Mission 4, Component 1 (CUP: F53D23009670001). Additional support was provided by the project ROADMAP funded under the PRIN 2022 call by the European Union – NextGenerationEU, Mission 4, Component 1 (CUP: F53D23001510006).

Data availability

Data will be made available on request.

References

[1] L. Al-Ghussain, Global warming: review on driving forces and mitigation, Environ. Prog. Sustain. Energy 38 (2019) 13–21.
[2] J. Barrett, T. Cooper, G.P. Hammond, N. Pidgeon, Industrial energy, materials and products: UK decarbonisation challenges and opportunities, Appl. Therm. Eng. 136 (2018) 643–656.
[3] T. Haasz, J.J. Gomez Vilchez, R. Kunze, P. Deane, D. Fraboulet, U. Fahl, E. Mulholland, Perspectives on decarbonizing the transport sector in the EU28, Energy Strategy Rev. 20 (2018) 124–132.
[4] X. Pan, H. Wang, L. Wang, W. Chen, Decarbonization of China's transportation sector: in light of national mitigation toward the Paris agreement goals, Energy 155 (2018) 853–864.
[5] A. Valera-Medina, H. Xiao, M. Owen-Jones, W.I.F. David, P.J. Bowen, Ammonia for power, Prog. Energy Combust. Sci. 69 (2018) 63–102.
[6] P.J. Feibelman, R. Stumpf, Comments on potential roles of ammonia in a hydrogen economy-a study of issues related to the use of ammonia for onboard vehicular hydrogen storage, Sandia Natl. Lab. (2006).
[7] A. Valera-Medina, F. Amer-Hatem, A. Azad, I. Dedoussi, M. de Joannon, R. Fernandes, P. Glarborg, H. Hashemi, X. He, S. Mashruk, Review on ammonia as a potential fuel: from synthesis to economics, Energy Fuels 35 (2021) 6964–7029.
[8] P. Dimitriou, R. Javaid, A review of ammonia as a compression ignition engine fuel, Int. J. Hydrogen Energy 45 (2020) 7098–7118.
[9] Z.A. Shah, et al., A review of recent studies and emerging trends in plasma-assisted combustion of ammonia as an effective hydrogen carrier, Int. J. Hydrogen Energy 51 (2024) 354–374.
[10] O. Mathieu, E.L. Petersen, Experimental and modeling study on the high-temperature oxidation of Ammonia and related NOx chemistry, Combust. Flame 162 (2015) 554–570.
[11] Y. Song, H. Hashemi, J.M. Christensen, C. Zou, P. Marshall, P. Glarborg, Ammonia oxidation at high pressure and intermediate temperatures, Fuel 181 (2016) 358–365.
[12] L. Dai, S. Gersen, P. Glarborg, H. Levinsky, A. Mokhov, Experimental and numerical analysis of the autoignition behavior of NH_3 and NH_3/H_2 mixtures at high pressure, Combust. Flame 215 (2020) 134–144.
[13] R. Lamioni, A. Mariotti, M.V. Salvetti, C. Galletti, Chemical reactor network modeling of ammonia–hydrogen combustion in a gas turbine: stochastic sensitivity analysis, Appl. Therm. Eng. 244 (2024) 122734.
[14] E.S. Rashed, A.E. Elwardany, M. Emam, S. Abo-Elfad, S. Mori, H. Hassan, 3D numerical study of NH_3/H_2 MILD combustion in a reversed flow MILD combustion furnace, Appl. Therm. Eng. 252 (2024) 123610.
[15] S. Wang, Z. Wang, A.M. Elbaz, X. Han, Y. He, M. Costa, A.A. Konnov, W.L. Roberts, Experimental study and kinetic analysis of the laminar burning velocity of NH_3/syngas/air, NH_3/CO/air and NH_3/H_2/air premixed flames at elevated pressures, Combust. Flame 221 (2020) 270–287.
[16] A. Jamrozik, W. Tutak, The impact of ammonia and hydrogen additives on the combustion characteristics, performance, stability and emissions of an industrial DF diesel engine, Appl. Therm. Eng. 257 (2024) 124189.
[17] J. Li, H. Huang, N. Kobayashi, C. Wang, H. Yuan, Numerical study on laminar burning velocity and ignition delay time of ammonia flame with hydrogen addition, Energy 126 (2017) 796–809.
[18] J. Choe Wenting Sun, T. ombrello, C. Carter, Plasma assisted ammonia combustion: simultaneous NOx reduction and flame enhancement, Combust. Flame 228 (2021) 430–432.
[19] G.T. Kim, J. Park, S.H. Chung, C.S. Yoo, Effects of non-thermal plasma on turbulent premixed flames of ammonia/air in a swirl combustor, Fuel 323 (2022) 124227.
[20] Y. Tang, D. Xie, B. Shi, N. Wang, S. Li, Flammability enhancement of swirling ammonia/air combustion using AC powered gliding arc discharges, Fuel 313 (2022) 122674.
[21] G. Faingold, J.K. Lefkowitz, A numerical investigation of NH3/O2/He ignition limits in a non-thermal plasma, Proc. Combust. Inst. 38 (2021) 6661–6669.
[22] A. Shioyoke, J. Hayashi, R. Murai, N. Nakatsuka, F. Akamatsu, Numerical investigation on effects of non-equilibrium plasma on laminar burning velocity of ammonia flame, EnergyFuels 32 (2018) 3824–3832.
[23] T.S. Taneja, P.N. Johnson, S. Yang, Nanosecond pulsed plasma assisted combustion of ammonia-air mixtures: effects on ignition delays and NOx emission, Combust. Flame 245 (2022) 112327.
[24] X. Mao, H. Zhong, N. Liu, Z. Wang, J. Yiguang, Ignition enhancement and NO*x* formation of NH3/air mixtures by non-equilibrium plasma discharge, Combust. Flame 259 (2024) 113140.
[25] Pancheshnyi S, Eismann B, Hagelaar G J M and Pitchford L C 2008 Computer code ZDPlasKin (available at: www.zdplaskin.laplace.univ-tlse.fr).
[26] Lutz A E, Kee R J and Miller J A 1988 SENKIN: a FOR-TRAN program for predicting homogeneous gas phase chemical kinetics with sensitivity analysis Report No. SAND87-8248 (Sandia National Laboratories).
[27] L.G. Piper, Energy transfer studies on N_2(X 1Σ+g, v) and N_2(B 3Πg), J. Chem. Phys. 97 (1998) 270–275.
[28] R. Kee, J. Grcar, M. Smooke, J. Miller, E. Meeks, PREMIX: a fortran program for modeling steady laminar one-dimensional premixed flames, Sandia Rep. 143 (1985).
[29] M. Shahsavari, A.A. Konnov, A. Valera-Medina, M. Jangi, On nanosecond plasma-assisted ammonia combustion: effects of pulse and mixture properties, Combust. Flame 245 (2022) 112368.
[30] H. Zhong, X. Mao, A. Rousso, C. Patrick, C. Yan, W. Xu, Q. Chen, G. Wysocki, Y. Ju, Kinetic study of plasma-assisted n-dodecane/O2/N2 pyrolysis and oxidation in a nanosecond-pulsed discharge, Proc. Combust. Inst. 38 (4) (2021) 6521–6531.
[31] "Dutton database," www.lxcat.net, December 13, 2021.
[32] B. Mei, X. Zhang, S. Ma, M. Cui, H. Guo, Z. Cao, Y. Li, Experimental and kinetic modeling investigation on the laminar flame propagation of ammonia under oxygen enrichment and elevated pressure conditions, Combust. Flame 210 (2019) 236–246.
[33] P. Sabia, M.V. Manna, A. Cavaliere, R. Ragucci, M. de Joannon, Ammonia oxidation features in a jet stirred flow reactor. The role of NH2 chemistry, Fuel 276 (2020) 118054.
[34] H. Hashemi, J.M. Christensen, S. Gersen, P. Glarborg, Hydrogen oxidation at high pressure and intermediate temperatures: experiments and kinetic modeling, Proc. Combust. Inst. 35 (2015) 553–560.
[35] P. Marshall, P. Glarborg, Probing high-temperature amine chemistry: is the reaction $NH_3 + NH_2 \rightleftarrows N_2H_3 + H_2$ important? Chem. A Eur. J. 127 (2023) 2415–2670.
[36] D.F. Davidson, K. Kohse-Hoinghaus, AY. Chang, RK. Hanson, A pyrolysis mechanism for ammonia, Int. J. Chem. Kinet. 22 (1990) 513–535.
[37] T.L. Nguyen, J.F. Stanton, Ab initio thermal rate coefficients for $H+NH_3 \rightleftharpoons H_2+NH_2$, Int. J. Chem. Kinet. 51 (2019) 321–328.

[38] A. Stagni, C. Cavallotti, S. Arunthanayothin, Y. Song, O. Herbinet, F. Battin-Leclerc, et al., An experimental, theoretical and kinetic-modeling study of the gas-phase oxidation of ammonia, React. Chem. Eng. 5 (2020) 696–711.
[39] S.J. Klippenstein, L.B. Harding, B. Ruscic, R. Sivaramakrishnan, N.K. Srinivasan, M.-C. Su, et al., Thermal decomposition of NH_2OH and subsequent reactions: ab initio transition state theory and reflected shock tube experiments, J. Phys. Chem. A 113 (2009) 10241–10259.
[40] D.L. Baulch, C.T. Bowman, C.J. Cobos, R.A. Cox, T. Just, J.A. Kerr, et al., Evaluated kinetic data for combustion modeling: supplement II, J. Phys. Chem. Ref. Data 34 (2005) 757–1397.
[41] P. Glarborg, J.A. Miller, B. Ruscic, S.J. Klippenstein, Modeling nitrogen chemistry in combustion, Prog. Energy Combust. Sci. 67 (2018) 31–68.
[42] Chemical-kinetic mechanisms for combustion applications, University of California at San Diego (2018). http://web.eng.ucsd.edu/mae/groups/combustion/ mechanism.html.
[43] Y. Zhang, O. Mathieu, E.L. Petersen, G. Bourque, H.J. Curran, Assessing the predictions of a NOx kinetic mechanism on recent hydrogen and syngas experimental data, Combust. Flame 182 (2017) 122–141.
[44] N. Cohen, K.R. Westberg, Chemical kinetic data sheets for high-temperature reactions. Part II, J. Phys. Chem. Ref. Data 20 (1991) 1211–1311.
[45] M.R. Talipov, S.L. Khursan, R.L. Safiullin, RRKM and ab initio investigation of the NH (X) oxidation by dioxygen, J. Phys. Chem. A 113 (2009) 6468–6476.
[46] M. Abian, M.U. Alzueta, P. Glarborg, Formation of NO from N_2/O_2 mixtures in a flow reactor: toward an accurate prediction of thermal NO, Int. J. Chem. Kinet. 47 (2015) 518–532.
[47] R. Sumathi, D. Sengupta, M.T. Nguyen, Theoretical study of the H_2+NO and related reactions of [H_2NO] isomers, J. Phys. Chem. A 102 (1998) 3175–3183.
[48] S.J. Klippenstein, L.B. Harding, P. Glarborg, J.A. Miller, The role of NNH in NO formation and control, Combust. Flame 158 (2011) 774–789.
[49] J.A. Miller, C.T. Bowman, Mechanism and modeling of nitrogen chemistry in combustion, Prog. Energy Combust. Sci. 15 (1989) 287–338.
[50] S. Inomata, N. Washida, Rate constants for the reactions of NH_2 and HNO with atomic oxygen at temperatures between 242 and 473 K, J. Phys. Chem. A 103 (1999) 5023–5031.
[51] M.E. Fuller, C.F. Goldsmith, On the relative importance of HONO versus HNO_2 in low-temperature combustion, Proc. Combust. Inst. 37 (2019) 695–702.
[52] S. Xu, M.C. Lin, Ab initio chemical kinetics for the NH_2+ HNO_x reactions, Part I: kinetics and mechanism for NH_2+ HNO, Int. J. Chem. Kinet. 41 (2009) 667–677.
[53] T. Varga, C. Olm, T. Nagy, I.G. Zsély, É. Valkó, R. Pálvölgyi, H.J. Curran, T. Turányi, Development of a joint hydrogen and syngas combustion mechanism based on an optimization approach, Int. J. Chem. Kinet. 48 (2016) 407–422.
[54] S.J. Klippenstein, R. Sivaramakrishnan, U. Burke, K.P. Somers, H.J. Curran, L. Cai, et al., H O_2 + H O_2: High level theory and the role of singlet channels, Combust. Flame (2022) 111975.
[55] A. Konnov, On the role of excited species in hydrogen combustion, Combust. Flame 162 (2015) 3753–3770.
[56] Z.H. Wang, L. Yang, B. Li, Z.S. Li, Z.W. Sun, M. Aldén, K.F. Cen, A.A. Konnov, Investigation of combustion enhancement by ozone additive in CH_4/air flames using direct laminar burning velocity measurements and kinetic simulations, Combust. Flame 159 (2012) 120–129.
[57] C. Chen, Z. Wang, Z. Yu, X. Han, Y. He, Y. Zhu, et al., Experimental and kinetic modeling study of laminar burning velocity enhancement by ozone additive in NH_3 +O_2+N_2 and NH_3+CH_4/C_2H_6/C_3H_8+air flames, Proc. Combust. Inst. 39 (2023) 4237–4246.
[58] Z. Ali Shah, G. Marseglia, M.G. De Giorgi, Predictive models of laminar flame speed in $NH_3/H_2/O_3$/air mixtures using multi-gene genetic programming under varied fuelling conditions, Fuel 368 (2024) 131652.
[59] A.M. Starik, V.E. Kozlov, N.S. Titova, On the influence of singlet oxygen molecules on the speed of flame propagation in methane–air mixture, Combust. Flame 157 (2010) 313–327.
[60] J. Otomo, M. Koshi, T. Mitsumori, H. Iwasaki, K. Yamada, Chemical kinetic modeling of ammonia oxidation with improved reaction mechanism for ammonia/air and ammonia/hydrogen/air combustion, Int. J. Hydrogen Energy 43 (2018) 3004–3014.
[61] X. Han, M. Lubrano Lavadera, A.A. Konnov, An experimental and kinetic modeling study on the laminar burning velocity of $NH^{3+}N_2O^{+}$air flames, Combust. Flame 228 (2021) 13–28.
[62] E.C. Okafor, Y. Naito, S. Colson, A. Ichikawa, T. Kudo, A. Hayakawa, H. Kobayashi, Experimental and numerical study of the laminar burning velocity of CH_4−NH −air premixed flames, Combust. Flame 187 (2018) 185–198.
[63] A. Stagni, C. Cavallotti, H-abstractions by O_2, NO_2, NH_2, and HO_2 from H_2NO: theoretical study and implications for ammonia low-temperature kinetics, Proc. Combust. Inst. 39 (2023) 633–641.
[64] J. Chen, X. Jiang, X. Qin, Z. Huang, Effect of hydrogen blending on the high-temperature auto-ignition of ammonia at elevated pressure, Fuel 287 (2021) 119563.
[65] Krishna Prasad Shrestha et al. An experimental and modeling study of ammonia with enriched oxygen content and ammonia/hydrogen laminar flame speed at elevated pressure and temperature. Proceedings of the Combustion Institute. 38 (2021) 2163–2174.
[66] X. Mao, Q. Chen, A.C. Rousso, T.Y. Chen, Y. Ju, Effects of controlled non-equilibrium excitation on H_2/O_2/He ignition using a hybrid repetitive nanosecond and DC discharge, Combust. Flame 206 (2019) 522–535, https://doi.org/10.1016/j.combustflame.2019.05.027.



https://dspace.org/

Refined kinetic mechanism for modeling ammonia combustion in air assisted by nanosecond discharged plasma

Shah, Zubair Ali; Cinieri, Giacomo; Zhu, Mingming; Chandio, Muhammad Basit; De Giorgi, Maria Grazia

2025-12-01
Elsevier
https://doi.org/10.1016/j.applthermaleng.2025.128121
Shah ZA, Cinieri G, Zhu M, et al., (2025) Refined kinetic mechanism for modeling ammonia combustion in air assisted by nanosecond discharged plasma. Applied Thermal Engineering, Volume 280, December 2025, Article number 128121

Downloaded from a DSpace repository. https://dspace.org/